SCUOLA DI SCIENZE
Dipartimento di Chimica Industriale “Toso Montanari”

Corso di Laurea Magistrale in

Chimica Industriale

Classe LM-71 - Scienze e Tecnologie della Chimica Industriale

Computational study of 5-hydroxymethylfurfural electrocatalytic hydrogenation over Cu(111) and Ag(111)

Tesi di laurea sperimentale

CANDIDATO

Fabio Loprete

RELATORE

Chiar.mo Prof. Ivan Rivalta

CORRELATORE

Dr.ssa Carine Michel

Dr. Stephan N. Steinmann

Chiar.ma Prof.ssa Patricia Benito Martin

Anno Accademico 2022-2023

Table of Contents

Abstract

Among biomass-platform molecules, 5-hydroxymethylfurfural (HMF) plays an important role since its great potential in the production of industrial monomers and fuels. One of the most interesting molecules procuded from HMF is 2,5-bishydroxymethylfuran (BHMF), which can be used in relevant industrial polymerization processes, such as for polyethers and polyesters syntheses. In this context, the selective electrochemical hydrogenation (ECH) of HMF (HMF-ECH) to BHMF is gaining an increasing interest. This process uses milder conditions compared to the thermocatalytic one, operating at room temperature and pressure and avoiding the use of H_2 as a reactant. This makes such electrocatalytic process a promising sustainable route. The main challenge is to achieve a high faradaic efficiency and a good selectivity toward BHMF formation. Experimentally, it has been shown that using Ag electrocatalysts a higher conversion, selectivity, and faradaic efficiency is achieved than the case of Cu electrocatalysts [1] [2] [3]. Still, a better understanding of the reaction network is necessary to limit the generation of side products, in particular hydrofuroin (BHH) and humines, and to limit the overpotential applied. In the last decade, *ab-initio* modelling has proved its ability to give an insight into the catalytic active site and to elucidate catalyzed reaction mechanisms [4]. Using the computational hydrogen electrode (CHE) approach and the grand-canonical periodic density-functional theory (GC-DFT), this work investigates the conversion of HMF into BHMF, but also the possible side routes such the ones yielding to methylfurfural (MF) and methylfurfuryl alcohol (MFA) that involve C-O scissions, and hydrofuroin (BHH), which involves a C-C coupling. The computational investigations have been supported by the experimental data collected by our collaborators at the University of Bologna.

To address the competition between HER (hydrogen evolution reaction) and HMF-ECH, the hydrogen coverage as a function of the potential has been explored. A higher activity toward HER has been predicted for Cu compared to Ag, in accordance with the experimental evidences.

Subsequently an extended reaction network for HMF-ECH has been explored over Cu(111) and Ag(111) surfaces, including only the proton coupled electron transfer (PCET) mechanism. The energy profiles have been computed in both cases. CHE and GC-DFT performances have been compared, showing that GC-DFT is a necessary refinement of CHE for those reactive steps where an appreciable difference of the dipoles occurs between the product and the reactant, in agreement with previous evidences reported in literature [5] [6].

Similar thermodynamic overpotentials for BHMF formation have been found for both Cu and Ag. This evidence agrees with the experimental results, which show the same activity for Cu and Ag in HMF-ECH.

The conditions used in the laboratory (-1.3 V vs SCE, pH = 9.2) are far from the computed thermodynamical overpotential. The computed energy profiles show that MFA, MF, BHH and BHMF can be formed from both the metals in these conditions, in line with the experimental evidences.

Along the path towards BHMF, the formation of the intermediate **I02**, which is involved also in BHH production, is athermic on Ag(111) and exothermic on Cu(111). On both metals, the stabilization of **I02** decreases as the electrode potential become more anodic. Based just on thermodynamics considerations, this outcome suggests an explanation why less BHH and humines are formed and a higher selectivity toward BHMF is observed in the case of Ag(111). Moreover, our results indicate a simple criterion for *in silico* screening of catalysts for HMF selective ECH.

1 Introduction

1.1 Biomass-derived compounds

1.1.1 General framework

The last decades have been characterized by an increasing concern related to anthropogenic impact over the ecosystems. The preservation of the environment has become an important part of political agenda. In this context, Industrial Chemistry can play a crucial role, with the development of more sustainable industrial processes. Although the adjective "sustainable" is often used improperly, its extension to Chemistry was scientifically defined by the American scientists Paul Anastas and John C. Warner. In 1998, they published the twelve principles of "Green Chemistry" [7], which is defined by the IUPAC as "the invention, design and application of chemical products and processes to reduce or eliminate the use and the production of harmful substances" [8]. The principles cover concepts as: avoiding the production of waste, designing of energy efficient processes, maximizing the incorporation of all materials in the final product, using of renewable material feedstocks and energy sources. In particular, the seventh principle states: "whenever is practical to do so, renewable feedstocks or raw materials are preferable to non-renewable ones" [7]. Following this goal, the concept of biorefinery emerged. In analogy to the conventional oil refinery, biorefinery aims the conversion of biomass and renewable feedstocks into fuels and platform chemicals [9]. Although the production of chemicals and materials from biomass traces back before the beginning of the industrial era, only in the last decades, it increased its relevance [9].

Lignocellulosic biomass feedstocks are mainly made of hemicellulose (25%), cellulose (40%) and lignin (30%). These compounds are big polymers, with several functional groups and a high content, that make them interesting sources for high-value specialty chemicals. The first step for the chemical transformation of biomass feedstocks is their "deconstruction". The polymers, in fact, must be "cut" into smaller molecules via gasification, liquefaction or pretreatment/hydrolysis [9]. The cellulose and the hemicellulose are both polysaccharides, meaning that they are made of monosaccharide units. Although the former is a linear chain of linked D-glucose units (six-carbon sugar), the latter is a heteropolymer, that also contains D-pentose (five-carbon sugar). Levoglucosan, a useful intermediate for chiral polymers synthesis, can be obtained from them. Furanics, like furfural, MF and HMF, can be formed, using the five or six-carbon sugar units. Finally, light oxygenates can be produced too. The lignin, instead, is a heteropolymer made by cross-linking of phenolic units. This feature makes it an interesting source of oxygenated aromatics (**Figure 1.1**).

Once the biomass-feedstocks are deconstructed into chemical building blocks, these ones must undergo other chemical reactions to be transformed into the desired molecules. This synthesis/upgrading process can be done in different ways. Photocatalytic, biological (anaerobic digestion, fermentation, microbiological fuel cells), thermal and electrochemical [9] transformations, each with their own opportunities and challenges, have been described in literature.

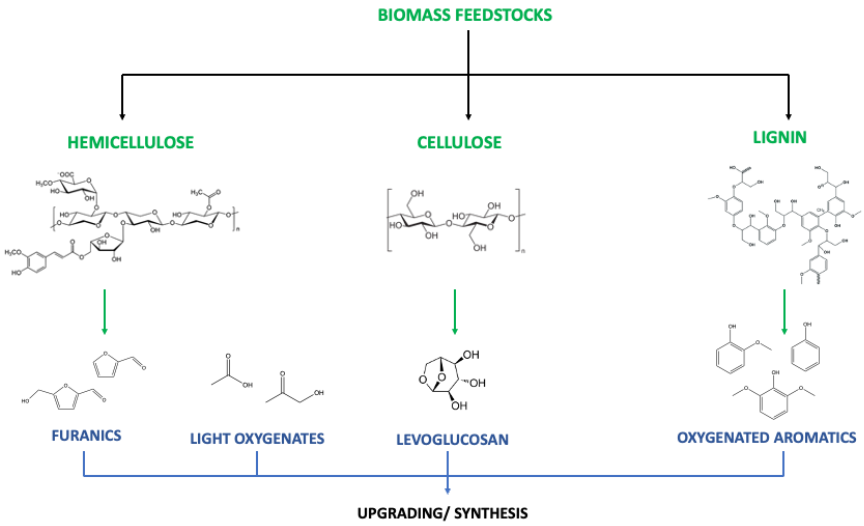

Figure 1.1. The products in green are the main constituents of the biomass feedstocks. The ones in blue, instead, are the ones directly produced from them. These chemical compounds can undergo further upgrading or synthesis processes.

1.1.2 Furanic compounds

Among the most promising biomass-derived compounds there are the furanics [9] [10]. These molecules are characterized by the presence of a furanic ring (i.e. a five-member aromatic ring, with one oxygen), that can have some branches with oxygenated functional groups. Within the furanics, furfural and HMF have attracted increasing attention [10]. The former presents an aldehyde function directly linked to the furanic ring. It is mainly obtained through the hydrolysis and dehydration of agricultural byproducts and the cyclodehydration of xylose [9]. HMF has a similar structure to furfural, but it has a -CH_2OH group in a specular position to the carbonyl. It is mainly formed from acid-catalyzed dehydration of pentose and hexose sugars [9].

The upgrading reactions of furfural and HMF have been extensively studied with experimental techniques, but also an ever increasing number of computational studies has been published,

showing a great interest [11] [12] [13]. HMF, in fact, has been defined a “sleeping giant” [14] because of its enormous synthetic and marketing potential for sustainable chemical industry in future. The products formed from its oxidation, hydrogenation and hydrogenolysis have several applications and can substitute platform chemicals coming from non-renewable fossil resources. For example, oxidating both the functional groups of HMF (i.e. carbonyl and hydroxyl groups) a dicarboxylic acid, called 2,5-furandicarboxylic acid (FDCA) is formed that can substitute petrochemical monomers (e.g. terephthalic acid) for the production of polyesters. Also, in the case of hydrogenation and hydrogenolysis high value-added compounds are produced. They can be exploited for the synthesis of fine chemicals, plastics, pharmaceuticals and liquid fuels (**Figure 1.2**). For example, 2,5-methylfuran (DMF) is a potential transportation fuel with high energy density. Also, side products, coming from electrochemical hydrogenation, like the dimer BHH, can find their applications as a jet fuel precursor [15]. However, among the hydrogenation products, 2,5-bishydroxymethylfuran (BHMF) is the most attractive one. In fact, it has peculiar symmetrical structure and wide potential applications in drug synthesis, as solvent or as a monomer for the production of polyesters, polyurethane foams, and resins [10].

All the high-value compounds described above are gaining attention from chemists because of two reasons: their promising applications and their production from renewable feedstocks. However, this last feature is not enough to make the overall production (from biomass feedstock to platform chemical) “sustainable”. In fact, all the principles of Green Chemistry must be respected along the reaction path. Upgrading reactions can then be crucial. Electrocatalytic conversion is gaining more attention in the last years, since it often requires milder conditions, that agree well with the principles of Green Chemistry and avoid the use of H_2 as the hydrogenating reactant in hydrogenation. Moreover, it can be powered with renewable energy and store it.

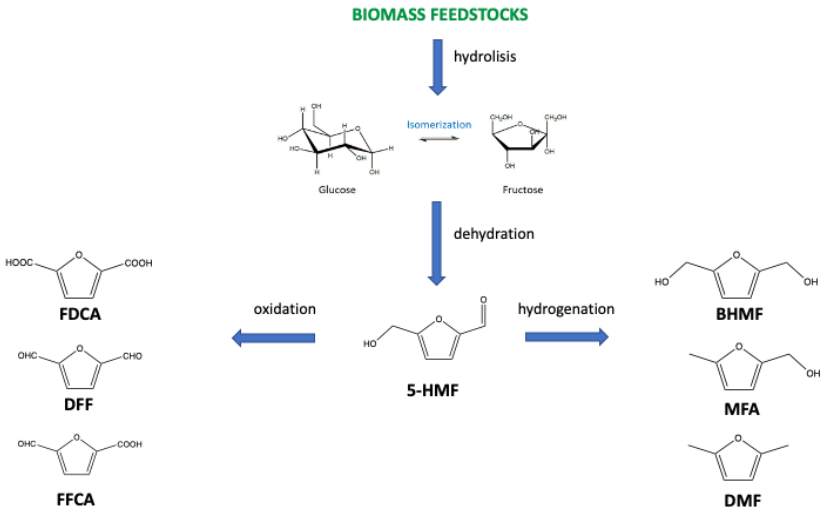

Figure 1.2. The main path from biomass feedstocks to HMF and some promising upgrading processes of it are shown. On the left, the most interesting oxidation platform molecules are represented, on the right the hydrogenation ones.

1.2 Electrocatalytic hydrogenation (ECH) of HMF

One of the most common upgrading transformations for bio-mass derived compounds is their hydrogenation. By increasing the H:C ratio, high quality fuels can be produced, while by decreasing the O:C ratio, the stability of the fuels and chemicals is improved [9]. This is true also for HMF, whose hydrogenated products have several applications. The conventional way in which the hydrogenation is performed is the thermocatalytic one, which requires quite high pressure and temperature. Furthermore, it uses H_2 as the hydrogenating reactant, with all the issues related to its production and use. In this context, the electrocatalytic hydrogenation (ECH) has promising features to be alternative to thermocatalytic transformations. This process, in fact, uses electrons instead of H_2 as reductant, and water as a source of hydrogen, avoiding the need of high H_2 pressures. Furthermore, it is usually performed at room temperature and pressure, avoiding costly heat integration [9]. Thus, renewable energetic sources can be exploited to produce the electricity needed *via* a sustainable process.

The following two sections collect the results reported in the literature for the HMF-ECH process and the experimental results obtained by the group of Prof. Patricia Benito Martin at the University of Bologna, which are the starting point of this work of thesis.

1.2.1 Experimental evidence on HMF-ECH: state-of-the-art

Several studies have been reported about HMF-ECH, aiming to find the best set-up to obtain the desired products. This reaction can produce different interesting products: BHMF, DMF, MFA, MF, BHH (**Figure 1.3**), among which BHMF has the most promising applications.

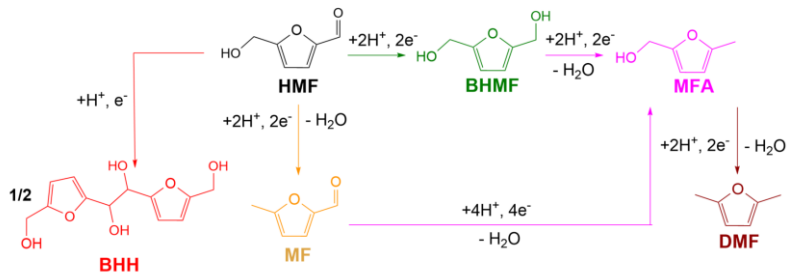

Figure 1.3. Products formed from electrocatalytic hydrogenation of HMF

Type of the solvent, pH, initial concentration of the reactant, and potential applied would greatly affect the selectivity towards BHMF and the faradaic efficiency. The electrode materials, the electrode support, and the electrode microstructure impact on the results too. For example, it has been found that metals like Co or Fe favor the hydrogenolysis (i.e. the formation of DMF), while for Ag and Cu the hydrogenation has a major impact (i.e. the formation of BHMF) [16]. When using Cu catalyst, the contribution of hydrogenation can become more important than hydrogenloysis, increasing the pH of the solution in which the reaction is performed [17]. Using Ag, the performance becomes better. The group of Prof. P. Benito Martin showed that, exploiting Ag foam, in a borate buffer (pH =9.2), at a low concentration of the reactant (0.02 M), at a potential of -1.30 V vs SCE, a conversion of 90%, a selectivity for BHMF of 75% and a faradaic efficiency around 60% are reached, when a charge of 96.5 Coulomb (i.e. the charge to theoretically reduce all the 0.02 M HMF to BHMF considering a 100% FE) has been accumulated (**Figure 1.4.a**) [1]. In the same conditions, for Cu foam a conversion of 80%, a selectivity of only 35% and a faradaic efficiency of 45% are reached (**Figure 1.4.a**). It has been observed that the selectivity and the productivity towards BHMF formation increase more when AgCu catalyst supported by Cu foam are used, in a basic media (i.e. borate buffer, pH = 9.2) [17] [2] [3] [1]. A conversion near to 100% and a selectivity around 80% are reached in this case (**Figure 1.4.a**) [1]. However, the origin of this performance improvement is not clear. Using higher concentration, the formation of the BHH dimer and oligomers reduces the selectivity, while more anodic potential favors also the hydrogen evolution reaction (HER) that reduces the faradaic efficiency (**Figure 1.4.b**) [1].

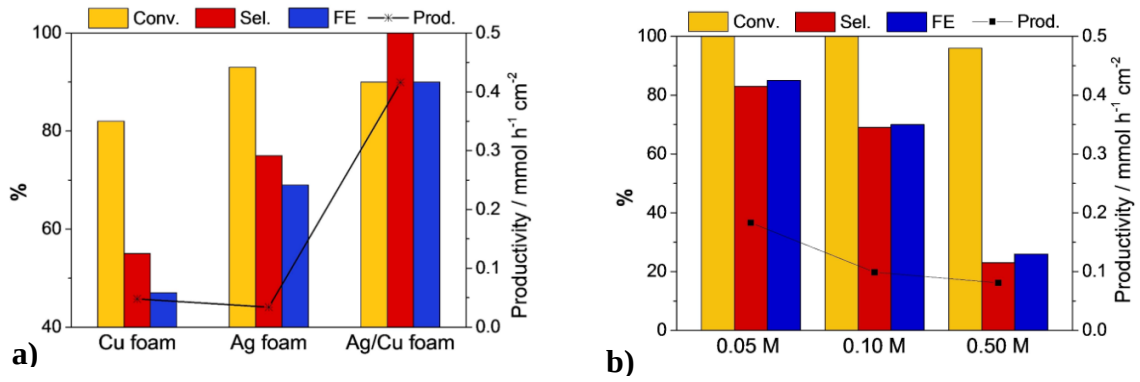

Figure 1.4 The experimental data collected by P. Benito Martin et al. for HMF-ECH are shown [1]. The histogram **(a)** shows the results for the ECH of a 0.02 M HMF solution in a borate buffer at -1.3 V vs SCE over Ag, Cu and Ag/Cu electrocatalyst. The histogram **(b)** shows the result for the reaction in a borate buffer at -1.3 V vs SCE over Ag/Cu electrocatalyst varying HMF concentration.

Another important issue related to HMF electrocatalytic reduction is the absence of a clear mechanistic insight. In fact, for both furfural and HMF-ECH, two types of mechanisms have been proposed: hydrogen adsorbed transfer (HAT) and proton-coupled electron transfer (PCET) [17] (**Figure 1.5**). In the first case one proton, coming from the electrolyte, receives an electron from the electrode surface and is adsorbed over the metallic surface (i.e. Volmer step). Then it is transferred to the adsorbed organic molecule. In the second case the proton is directly transferred to the molecule from the electrolyte and the electron directly comes from the charged electrode surface. In the case of furfural, X. H. Chadderdon and his collaborators distinguished through experimental techniques the type of mechanism involved [18]. They found that using Cu catalyst in acidic conditions both the types of mechanism happen. In particular, the alcohol (FA) and the hydrogenolysis product (MF) seem to be formed from HAT mechanism. At the best of our knowledge, similar experimental studies have not been performed for HMF yet. Knowing what type of mechanism is involved could drive the choice of the best set up for the reaction, and computational chemistry could be certainly of great help.

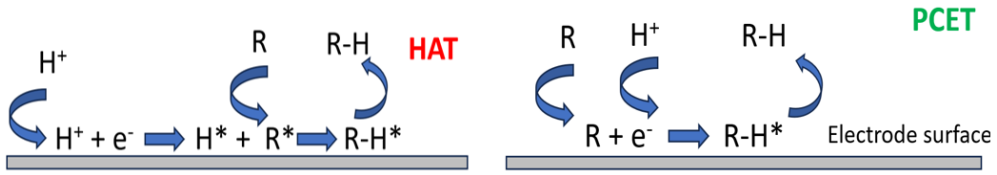

Figure 1.5. Two mechanism proposed for ECH. On the left the HAT mechanism, on the right the PCET mechanism. “R” indicates the generic organic molecule, and “R-H” is the hydrogenated species. "*" indicates adsorbed species.

1.2.2 Supporting experimental evidences

This thesis combines experimental and computational evidences, aiming to elucidate the mechanism of HMF electrocatalytic hydrogenation over different catalysts, in a borate buffer (pH = 9.2). The experimental data that support this work have been collected by the group of Prof. Patricia Benito Martin at the Department "Toso Montanari" of the University of Bologna. Three types of catalysts have been prepared through electrodeposition: Cu/Cu foam, Ag/Ag foam and Ag/Cu foam. Bare Ag and Cu foams have not been considered since they have a lower electroactive surface area than Ag/Cu foam.

The performance of each catalyst was then tested. Linear sweep voltammetry (LSV) was performed to evaluate the onset potential of HER and the one of HMF-ECH. Measurements were firstly made on the borate buffer alone (pH = 9.2), showing an onset potential of -1.1 V vs SCE for Cu/Cu foam, of -1.2 V vs SCE for Ag/Ag foam, and -1.15 V vs SCE for Ag/Cu foam (**Figure 1.6.a**). These data confirm that both the metals are poor HER catalysts and good candidates for the HMF-ECH. Cu is more active than Ag foam in agreement with results collected in literature [17]; HER starts at ca. 100 mV lower overpotential and the current density increases faster at more cathodic potential. Other tests were performed on a 0.1 M solution of HMF (**Figure 1.6.b**). The onset of the peak for HMF reduction is recorded at -1.1 V vs SCE vs SCE for Cu/Cu foam and Ag/Ag foam, and around -1.05 V vs SCE for Ag/Cu foam. These data suggest that the monometallic catalysts have the same activity in HMF conversion, while the bimetallic ones show a slightly improved behavior compared to them. The potential onsets are more anodic than the ones of HER for all the catalysts, meaning that there is a potential window in which a strong competition between HER and HMF-ECH can be avoided.

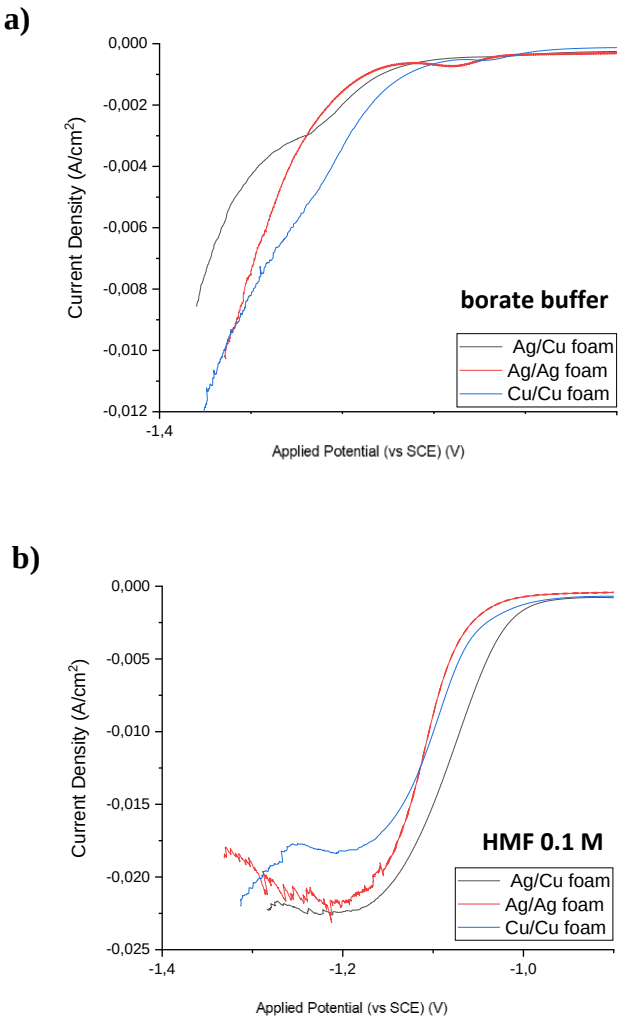

Figure 1.6. The LSV tests for borate buffer **(a)** and for a solution of HMF 0.1 M **(b)**. The blue profile refers to Cu/Cu foam catalyst, while the red one refers to Ag/Ag foam catalyst and the grey one refers to Ag/Cu foam catalyst.

For each catalyst the reaction has been studied at -1.30 V vs SCE, in a borate buffer (pH = 9.2). A concentration of HMF 0.1 M was used. These conditions have been chosen as standard experimental ones, although it has been previously shown that more diluted solutions show better performances. Some samples have been picked-up during the reaction, for all the three catalysts, and analyzed with HPLC. This analysis tracks the conversion of HMF and the selectivity of each product as a function of the time or of the accumulated charge (**Figure 1.7**). For each catalyst, high conversion of the reactant is reached at the stoichiometric charge required for the full conversion of HMF/BHMF (482.4 Coulomb), assuming unitary faradaic efficiency and selectivity. The slope of the conversion profiles is quite similar for each catalyst, suggesting similar kinetics. In the case of Cu electrocatalyst, BHMF selectivity reaches rapidly a plateau at 43%. Ag electrocatalyst shows a constant and higher BHMF selectivity at 81%. In

contrast, BHH selectivity always decreases, reaching a 17% for Cu and a 13% for Ag at the end of the reaction. Ag/Cu foam, instead, shows an intermediate behavior with its monometallic counterparts, for both BHMF selectivity, that is constant around 73% and BHH selectivity, which always decreases and reaches a 14% at the end of the reaction. MFA selectivity remains quite constant during the reaction, and for Ag/Cu foam and Cu/Cu foam it shows a small increasing at high accumulated charge. It reaches a 3% for Cu catalyst and a 1% for Ag catalyst at the end of the reaction. MF shows a similar behavior, with a selectivity that remains always below 1% for the three catalysts.

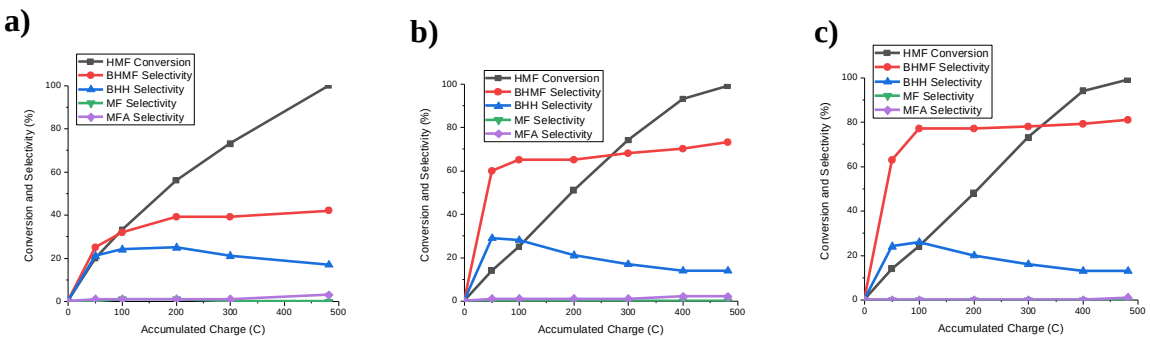

Figure 1.7. The experimental conversion and selectivity profiles plotted against the accumulated charge for HMF-ECH. The plots refer to **(a)** Cu/Cu, **(b)** Ag/Cu and **(c)** Ag/Ag foam catalysts. The reaction has been performed at pH = 9.2 with an applied electrode potential of -1.30 V vs SCE and a concentration 0.1 M of HMF.

The conversion of HMF and the selectivities towards the formation of each product at an accumulated charge of 482.4 Coulomb (i.e. the stoichiometric charge) are shown in **Figure 1.8**. As for the definition of conversion and selectivity, the sum of each product selectivity must be equal to the conversion. A percentage of 34% is lost for Cu/Cu foam, while for Ag/Ag foam it is just a 4% (that can be considered within the experimental error), and for Ag/Cu foam it is an intermediate value of 10%. In literature, it has been suggested that this carbon loss is due to humines, that are formed by oligomerization [16] [17] [2]. Such as the process of dimerization happens, with the formation of BHH, it is possible that longer molecular chains can be formed. These chains can be formed possibly from BHH. As shown in **Figure 1.7**, BHH selectivity always decreases as a function of the accumulated charge. BHH formation is a dimerization process and requires C-C coupling of two intermediates. As soon as HMF decreases this process becomes less probable, possibly explaining the decrease of selectivity. The decrease can also possibly be ascribed to the oligomerization process, starting from BHH. Humines have been observed for furfural and benzaldehyde [19]. High molecular weight compounds have

been identified also in our experimental conditions, although they have not been quantified and characterized [1].

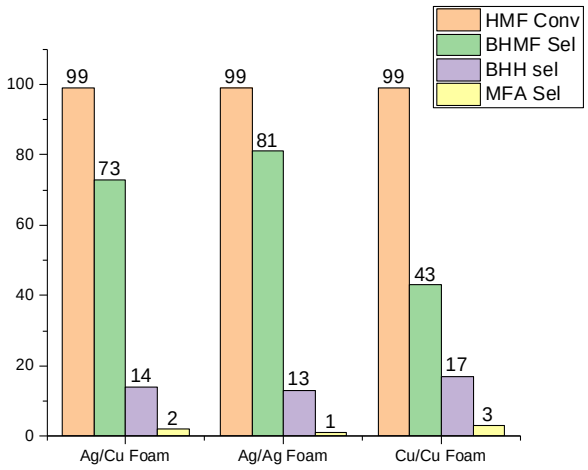

Figure 1.8. The conversion of HMF (orange bar) and the selectivities for BHMF (green bar), BHH (purple bar) and MFA (yellow bar) are shown for the three catalysts used. The data refers to the electroreduction of HMF at -1.30 eV vs SCE in a pH = 9.2 borate buffer with HMF 100 mM at 482.4 Coulomb transferred.

In conclusion, among the three catalysts Ag/Ag foam is the one that displays the best performance in selective HMF hydrogenation to BHMF. It shows a high BHMF selectivity, that is almost the double of the one shown by Cu/Cu foam. Also, BHH selectivity is lower for Ag/Ag foam compared to Cu/Cu foam, and only traces of MFA are revealed. For all products selectivities, Ag/Cu foam displays an intermediate behavior between the monometallic counterparts. A greater carbon loss is found for Cu/Cu foam compared to Ag/Ag foam, probably due to humines formation, in agreement with the results collected by other research groups [16]. Possibly, the oligomerization process starts from BHH, since it shows a decreasing selectivity for all the catalysts. In order to address the reason behind the increase in selectivity moving from Cu to Ag electrocatalysts, the reason behind a different trend in the humines formation should be clarified.

1.3 Electrocatalysis

1.3.1 Fundamental aspects

Electrocatalysis can be simply defined as “an electrochemical reaction that takes advantage of a catalyst” [20]. Despite this simple definition, electrocatalysis hides several complications.

Two kinds of processes can be distinguished when considering an electrochemical phenomenon: inner sphere processes, in which an electron transfer is accompanied by the formation/breaking of chemical bonds, and outer sphere processes in which only electron transfers happen [21]. Since a catalyzed reaction is made up of several reactive steps, a combination of inner sphere, outer sphere and “pure” chemical steps is possible. Electrochemical reactions (i.e. redox reactions) are the combination of two half-reactions: oxidation and reduction. As every type of reaction, they can be spontaneous or not. In the second case they need an external power source (i.e. electrolytic cell), meaning that an electrode potential must be applied. In a simplified picture, two electrodes can be considered as the places where each of the two half-reactions occur. The electrode is therefore, a charged surface, with which the reactant molecules can interact, and it is the catalyst in an electrochemical reaction. For this reason, the choice of the electrode material and also of the electrode potential can increase the reaction rate. A good catalyst also drives the reaction towards the desired products, limiting the side reactions, increasing selectivity and faradaic efficiency. The first parameter refers to the amount of a certain product formed relative to the amount (moles) of the reactant consumed. The second one, instead, is the amount (moles) of collected product relative to the amount that could be produced from the total charge passed, expressed as a fraction or a percent.

The following discussion is focused on the phenomena that happen near to one electrode (i.e. one half-reaction). The electrocatalyst is a solid surface. It is usually surrounded by a liquid environment, that consists in solvent, reactant molecules and other substances (e.g. soluble salts). All these components constitute the electrolyte. A solid/electrolyte interface is then formed, and it is crucial in driving the electrochemical reaction. A microscopic model that describes the interface is the electrical double layer (EDL) (**Figure 1.9**) [21]. In order for the interface to remain neutral, the charge held on the electrode must be balanced by the distribution of ions close to the surface. The ions with an opposite charge approach the surface and form a layer balancing the electrode charge. This region is called Outer Helmholtz Plane (OHP). The overall result is two layers of charge (the double layer) and a potential drop starting from the surface. However, it should be considered that the electrostatic interactions are in

competition with the Brownian motions. The ions are therefore temporary bound to the electrode surface and influenced by the thermal energy. The OHP is spatially followed by the diffuse layer, where the charges and their counterparts are collected; in this region their properties are slightly influenced by the charged surface. Finally, beyond the diffuse layer, there is the bulk where the properties of the electrolyte are not influenced anymore by the presence of the charged surface.

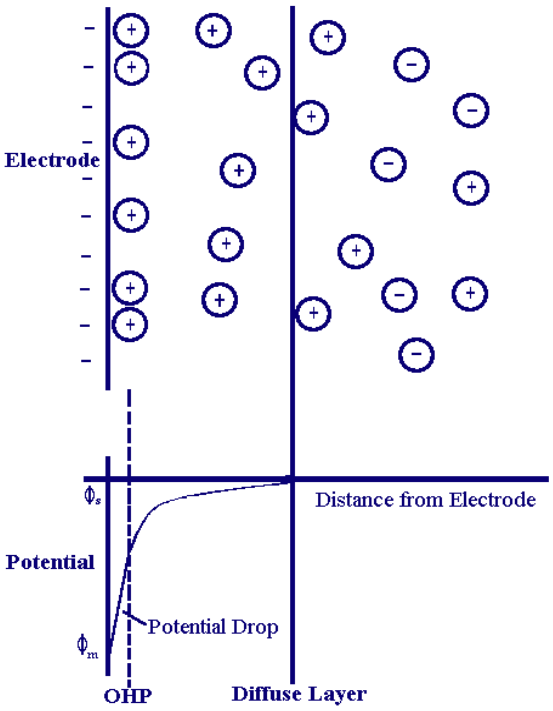

Figure 1.9. A representation of the electrical double layer (EDL) model is shown. Above, the blue line on the left represents the electrode surface, that is considered to be negatively charged. Moving to the right a spatial distribution of the ions (blue circles) is represented. The layer of cations near to the surface forms the OHP. The cations immediately on the right forms the diffuse layer. Moving more on the right, beyond the blue line the cations and anions form the bulk. Below, the variation of the potential as a function of the distance from the electrode is shown (https://www.ceb.cam.ac.uk/research/groups/rg-eme/Edu/the-electrical-double-layer)

In order to elucidate the role of the electrocatalyst, some thermodynamic considerations must be done. Each electrochemical reaction has a standard equilibrium potential U°, that is connected to the standard free reaction energy $\Delta G°$ [21]:

$$\Delta G° = -nFU° \qquad (\mathbf{1.1})$$

where n is the number of electrons that are exchanged and F is the Faraday's constant. A generalization of this equation is the wide known Nernst equation. From these relations, the

minimum cell potential, that is required to make the overall reaction spontaneous (i.e. $\Delta G \leq 0$) can be derived. However, the application of this potential, is not enough for the reaction to "happen". In fact, although the application of the electrode potential modifies the potential energy surfaces for the reactant and the product (and the intermediates too) and allow the reaction to become spontaneous from a thermodynamical point of view, also kinetics aspects must be considered. The difference between half-reaction's thermodynamically determined equilibrium potential and the potential that must be applied in order to make the redox event experimentally observable is called overpotential (η) [21]. Considering an electrolytic cell, the consequence of the overpotential is that more energy than thermodynamically expected is required to drive the reaction. There are three different types of overpotential: the concentration overpotential, the resistance overpotential and the activation overpotential. The first is due to a variety of phenomena that involve the depletion of charge-carrier at the electrode surface. The second is related to the cell design (i.e. electrolyte diffusion, surface polarization and other sources of electromotive forces). The third one is related to the activation barriers, whose energies impact on the reaction rate. It can be reduced or eliminated with the use of electrocatalysts. In this aspect lies the best description of electrocatalysis. An electrocatalyst lowers the activation barriers, reducing the potential that must be applied in order to increase considerably the rate reaction, that means a reduction of the overpotential applied (since the equilibrium potential, and the thermodynamics, are not influenced, as for the definition of "catalyst") [22].

A better comprehension on the role of the catalyst can be reached looking at the kinetics equation in electrocatalysis. In the following discussion only one reactive step is considered. Actually, the electrocatalyzed reaction is a reaction network, made of several steps, each with its own activation barrier, that can be electrochemical or purely "chemical" (i.e. an electron transfer is involved or not during the reactive step). One example of kinetic equation for electrochemical phenomena is the Butler-Volmer one. This relationship is derived for the special case of unimolecular redox half-reaction (i.e. inner sphere process) and relates electrical current density (j) with the applied electrode potential and therefore the overpotential (U, η) [21]. Consider the following reduction half-reaction:

$$ox + ze^{-} \rightarrow red \qquad (\mathbf{1.2})$$

The Butler-Volmer equation can be expressed as:

$$j = j_0 \left\{ \frac{c_{ox}(0,t)}{c_{ox*}} exp\left[\frac{\alpha_a z F \eta}{RT}\right] - \frac{c_{red}(0,t)}{c_{red*}} exp\left[-\frac{\alpha_c z F \eta}{RT}\right] \right\} \quad (\mathbf{1.3})$$

Considering a single electron transfer and neglecting mass-transfer issues (i.e. concentration is everywhere the same and equals the bulk value c_x*) the equation becomes [21]:

$$j = j_0 \left\{ exp\left[\frac{\alpha_a F \eta}{RT}\right] - exp\left[-\frac{\alpha_c z F \eta}{RT}\right] \right\} \quad (\mathbf{1.4})$$

where j is the electrical current density and it is related to the reaction rate through the Faraday's law. The higher is j, the higher is the reaction rate. Instead of the electrode potential, the overpotential (η), that is defined as the difference (U° - U), appears in the argument of the exponential. The first exponential term is referred to the direct reaction, while the second refers to the reverse one. Electrode potential influence therefore the kinetics and not only thermodynamic. The higher the electrode potential applied, the higher is the current density (i.e. reaction rate increases). Lastly, two important parameters appear in the equation: the charge transfer coefficient (α_x , called also symmetry factor) and the exchange current density (j_0). Both these quantities are specific of the catalyst. α_x is a factor used to define the activation barrier dependance on the potential [21] (**Figure 1.10**):

$$\Delta G^{\#}(U) = \Delta G^{\#}(U°) + \alpha n F U \quad (\mathbf{1.5})$$

Equation 1.5 is the greatest approximation inside Butler-Volmer equation; beyond its simplicity there are not evidences to make this assumption. In the derivation of the equation the energy profile near to the transition state is assumed to be linear, consequently the charge transfer coefficient is a constant. So, α_x can change with the catalyst, and together with the overpotential, affects the activation barrier. The exchange current density (j_0), instead, is the anodic respectively cathodic current density at the equilibrium. It is linked to the kinetic constant of the reaction, and therefore it is proportional to $exp\left[\frac{-\Delta G^{\#}(U)}{k_b T}\right]$. The lower the activation energy, the higher is the exchange current density. j_0 is the most crucial parameter for an electrocatalyst, since the symmetry factor usually doesn't change too much (it is often around 0.5) [23].

Better approximation leads to Marcus-Hush theory. In this context in fact, the energy profile is considered to be a parabola instead of a straight-line, resulting in a quadratic dependence of the current density toward the overpotential and, also, the presence of the electrolyte is taken into account someway (i.e. reorganization energy (λ)) [21].

However, Butler-Volmer equation is enough to understand the role of an electrocatalyst. It shows, in fact, that the catalyst impact on the transition state energy, lowering the overpotential needed to reach a certain current density. From this equation can be therefore concluded that the objective of electrocatalysis is to increase the exchange current density (j_0) for an electrochemical reaction by optimizing the electrode material.

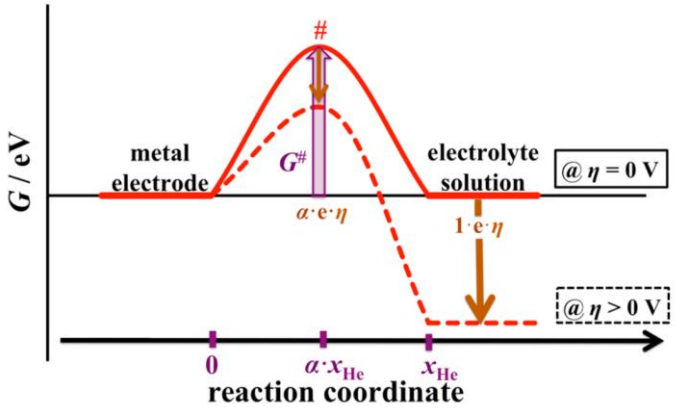

Figure 1.10. Free energy diagram of a single electron transfer between a metal electrode (e.g. Ag) and the electrolyte solution (e.g. Ag^+) within the Helmholtz double layer of thickness x_{He} is shown for two overpotentials $\eta = 0\,V$ (equilibrium) and $\eta > 0\,V$ (anodic polarization), adapted from [23].

1.3.2 Atomic scale modelling of electrocatalysis

Numerous variables can affect activity and selectivity in an electrocatalytic reduction: electrode material, electrode support, temperature, pH, but also electric field and electrode potential [11]. The effects of all these parameters must be carefully tested on a laboratory scale in order to find the best electrocatalyst and set up for the hydrogenation. In the last decades, computational chemistry has become a very useful tool to reduce the experimental efforts. *Ab initio* modelling, in fact, has proven its ability to rationalize the observed trends and to propose novel catalyst design, also for reactions involving biomass-derived compounds [4]. The two major advantages of computational investigations are the elucidation of the reaction mechanism and the deeper insight into catalytic active site [4]. Both these targets, in fact, are not easy to reach experimentally.

Catalysis is intrinsically a multiscale process, and atomic scale investigation should be combined with studies on a greater scale. In fact, phenomena like mass-transfer or charge transfer, that are dramatically scale dependent, impact on the overall kinetics [24]. However, atomic scale investigation is often enough to rationalize experimental data and to do *in silico* design of the catalyst. Starting from the definition of a hypothetical reaction network and performing computation at the DFT level of the corresponding reaction and activation energies, can give a useful insight into the reaction. Furthermore, the effects of some reaction variables can be selectively included into the theoretical modelling, decomposing the effect of each variable considered .

Computational heterogeneous electrocatalysis presents some additional complications to the ones typical of computational heterogeneous catalysis. In fact, an electrified surface and a solid/electrolyte interface must be modeled [24]. It is therefore necessary to consider the effect of the electrode potential over the energy profile, including, in principle, also the effect on the activation barriers. Furthermore, the presence of an electrolyte is also important, and it is necessary to include the "response" of the electrolyte to the applied potential (i.e. the change on atomic scale of the solid/electrolyte interface), meaning that the electric double layer must be theoretically reproduced. These aspects explain why many efforts have been concentrated on ab initio simulation of electrochemical reactions over the years.

J. Nørskov and his collaborators were the authors of a crucial turning point in atomic scale modelling of electrocatalysis. In 2004, the so-called "Computational Hydrogen Electrode" (CHE) was introduced to study the oxygen reduction over platinum [25]. Thanks to this approach the authors were able to identify the origin of the overpotential found for this important reaction. In the context of CHE, the presence of an electrified interface is not included in the quantum-mechanical (QM) calculation, but the effect of the electrode potential is introduced subsequently as a changing factor for the electrochemical potential of the couple ($H^+ + e^-$). This crucial quantity can be derived in a straightforward manner from the energy of the H_2 molecule in gas phase (see chapter 2) [25]. The effect of the electrode potential is therefore considered only for the reaction steps where ($H^+ + e^-$) is involved, and the effect on activation barrier is totally ignored. Although, in the article published in 2004 a monolayer of water molecule was explicitly included to consider the presence of the solvent, other studies that use the CHE approach usually ignore it [25] [26]. A quite simple method was therefore developed, and this explains why it became really popular during the years. Since the electrode potential effect on the activation barriers is not included in the method, CHE can be considered

as an *ab initio* thermodynamic approach [23]. This feature is quite bizarre, since catalysis is intrinsically a kinetic phenomenon and, in principle, kinetic information (i.e. activation barriers) are needed to compare different catalysts. However, CHE method has largely proven its ability in catalyst screening, without the consideration of full potential-dependent surface states and activation barriers. Assuming that the activation barrier scales with thermodynamics (i.e. the so called Bell-Evans-Polanyi, BEP, relation), and the kinetic part of the barrier is small, ab initio thermodynamics may provide atomic scale insights into the electrochemical reaction kinetics [23]. However, for many electrocatalytic reactions, these tacit assumptions are violated, so that thermodynamics will lead to contradictions with both experimental data and *ab initio* kinetics [23]. CHE approach could need sometimes refinement with other more costly approach.

Grand-canonical density functional theory (GC-DFT) is a possible solution to this problem. A DFT method that aims to model electrochemical phenomena, must consider that electrons can flow in and out of the electrode as electrochemical reactions proceed, meaning that a grand canonical (GC) ensemble is involved. There are different ways in which this can be modelled. One approach is to use some modified Kohn-Sham equations that are derived from the functional minimization, but with a constrain on the potential (i.e. potentiostatic conditions) instead of a constrain on the electron number (since they can change) [27]. Otherwise, without a control over the electrochemical potential value, different DFT calculations for the same systems but with a different electron number can be performed. Fitting the energy *versus* the electrochemical potential (that is evaluated only at the end of each calculation), a function is obtained, that allows to evaluate the energy of the system for the electrode potential of interest. Both approaches consider the presence of a charged surface into the QM calculation, and in principle can allow to evaluate the effect of the potential for all the types of reactive steps and also on the activation barriers. The method is implemented in codes involving periodic boundary conditions, which feature problems with charged systems, so different solutions have been extensively studied to make the entire cell neutral [26]. The solid/electrolyte interface must also be considered to reach a greater accuracy. While DFT has become the tool of choice to model both molecules and crystalline substrates, dealing with liquids using ab-initio simulations can be challenging, because of length-scales and time-scales. First-principles simulations of electrochemical systems with a fully explicit description of each component are usually beyond reach [28]. An alternative approach are the continuum models of solvation, in which solvent molecules are substitute by a polarizable medium. These approaches were first designed in combination with simulation packages based on localized basis sets, for the study

of isolated molecules and cluster. In the context of heterogeneous electrocatalysis, condensed-matter simulation codes are needed, since a solid surface must be included to simulate the electrode surface, where the molecules are adsorbed and react. One of the most interesting reformulations of continuum model in periodic codes is the Joint-density functional theory (JDFT). It was developed in 2005 by S. A. Petrosyan and his collaborators, at Cornell University, for "the ab initio description of electronic systems in contact with molecular liquid environment" [29]. They did not simple replace the electrolyte with an effective continuum material, but the atomic nature of the electrolyte was also considered using a statistically-averaged density for the atomic species in the solution [29]. They demonstrated that this approach was able to describe the Cr_2O_3 surface chemistry in solution [29]. In summary, this theoretical approach joins a classical DFT to describe the electrolyte with a standard electronic DFT for the reactive part, and for this reason it was called "Joint Density Functional Theory" (JDFT) [29]. Since the solute is still being treated quantum-mechanically, this approach can be quite accurate assuming all interactions between the solute and the solvent are considered in proper details. Following the framework of JDFT, Mathew at al. in 2014 developed and implemented an implicit solvation model that has a "firm theoretical foundation into the widely used density-functional code Vienna ab initio Software Package" [30], called VASPsol. This package provides an efficient approach for estimating the solvation effects for large periodic systems, but without using the statistically-averaged densities of solute species as JDFT does. In 2019, Mathew et al. extended the solvation model to include the effects of mobile ions in the electrolyte through the use of the linearized Poisson-Boltzmann equation [31]. The use of this equation also allows the overall system to be neutral, solving the problem of a charged surface calculation using periodic boundary conditions. Within VASPsol framework, GC-DFT is able to describe the presence of a charged surface and the solid/electrolyte interface. with a good compromise between the computational efforts and accuracy. The energy profiles, including transition states, can be therefore evaluated within this framework, going beyond the approximations of CHE.

An alternative methodology to the GC-DFT is the use of model Hamiltonians [26]. They combine Marcus' theory for electron transfers and the physical Anderson-Newns Hamiltonian for the interaction between the adsorbates and the electrode [32], allowing for the computation of the free energy surface. Without going into the details, the major strength of this method is a deeper insight into the electrochemical reactions, thanks to the three-dimensional energy surface generated. On the other hand, model Hamiltonians must be set up for each system specifically.

1.4 Scope of the thesis

This thesis is dedicated to a computational study of the electrocatalytic hydrogenation of HMF over Cu(111) and Ag(111). Experimental data collected by P. Benito and coworkers in the last three years showed improved performances in terms of selectivity, faradaic efficiency and productivity, for HMF selective ECH to BHMF, moving from Cu to Ag based electrocatalysts [1] [2] [3]. Still, experimental studies need the support of computational tools in order to clarify the reaction mechanism and the role of the catalyst active site. Combining the experimental data collected at the University of Bologna and our computational approach, this thesis aims to: 1) compare the performances of CHE and GC-DFT approaches in the study of HMF-ECH 2) elucidate the reaction mechanism over Cu(111) and Ag(111); 3) rationalize the experimental data; and 4) define the criteria for the design of better catalysts.

The main computational tool used is the VASP package for DFT calculations. The effect of the electrode potential is considered using first the CHE framework and then GC-DFT. In this work only PCET mechanism is considered inside the reaction networks.

The thesis is divided into five chapters: **Chapter 2** describes the main computational methodologies used; **Chapter 3** is dedicated to the computational details; **Chapter 4** collects the results and their discussion; finally, **Chapter 5** is dedicated to the conclusions and to the future outlooks for this thesis work.

2 Methodologies

2.1 VASP

2.1.1 General outlook

VASP (Vienna Ab Initio Simulation Package) is a widely used package for performing ab initio quantum mechanical calculations in the context of atomic scale materials modelling [33]. One of the most important features of this computer program is the use of a plane wave basis set, that is the most convenient choice in the case of three-dimensional periodic boundary conditions.

The basic methodology used by VASP is the DFT (Density Functional Theory), although also many-body perturbation theory and Green's functions methods have been implemented in the code. The following discussion is, however, focused on the DFT methodology, since it is the one used in this work. Among the functionals: LDA, GGA, meta-GGA, hybrid functionals and Van der Waals ones are supported by the code [34]. VASP solves the Kohn-Sham equations for a periodic system, allowing the evaluation of one-electron orbitals, their associated energies and the electronic charge density [33]. All the central quantities (e.g. one-electron orbitals, electronic charge density, local potentials) are expanded in plane wave basis set, instead of localized basis set (as the ones used in Gaussian for example) [33]. The reasons behind this choice lie in the periodic nature of the systems studied with VASP. From Bloch's theorem it is known that in presence of a periodic potential the solutions of the Schrödinger equation take the form of a plane wave multiplied for another periodic function, with the same periodicity of the system (**Equation 2.1**) [35]. It comes quite natural to choose a plane wave basis set to express the periodic function (**Equation 2.2**).

$$\psi_{nk}(r) = e^{ikr}\, u_{nk}(r) \qquad (\mathbf{2.1})$$

$$u_{nk}(r) = \frac{1}{\Omega^{1/2}} \sum_G C_{Gnk} e^{iGr} \qquad (\mathbf{2.2})$$

$$u_{nk}(r) = \frac{1}{\Omega^{1/2}} \sum_G C_{Gnk} e^{i(G+k)r} \qquad (\mathbf{2.3})$$

Equation 2.3 shows the general expression for a one-electron wavefunction, defined as a linear combination of plane waves [34]. Two indexes appear as subscripts. Since the system is periodic, the electronic structure is characterized by the presence of bands. The index "n" refers to the number of the band and "k" is a vector of the reciprocal space, that can be seen as a second quantum number. The choice of a plane wave basis set is also due to other computational reasons. The action of the Hamiltonian on the orbitals can be, in fact, efficiently evaluated using FFTs (Fast Fourier Transform) in this case [36]. The dimension of the basis set is defined by the energy cutoff (E_{cut}). All plane waves with a kinetic energy smaller than E_{cut} are included [34].

Although this basis set is a good choice to expand the wavefunction in the presence of a periodic potential, they are a bad choice to represent the behavior of the functions near to the nuclei, where they can have many nodes. In this case a very big plane wave basis set would be necessary. In summary, the main problem is that tightly bound states (spatially strongly localized) and rapid oscillations (near to the nuclei) should be managed together. In order to make the plane wave basis set efficient, some smart solutions must be introduced. Firstly, a frozen core approximation can be used. Since the core electrons are usually chemically inert, they are pre-calculated in an atomic environment and kept frozen during the remaining calculations [34]. Secondly, it is useful to substitute the exact potential with a pseudopotential. It means that the all-electron potential is replaced by an effective potential, that is able to represent the correct behavior in the interstitial region between the atoms, but not near to the nuclei (**Figure 2.1**) [34]. Using this approach, the valence electrons are described by pseudo-wavefunctions with significantly fewer nodes, making the plane-wave basis set an efficient one [34].

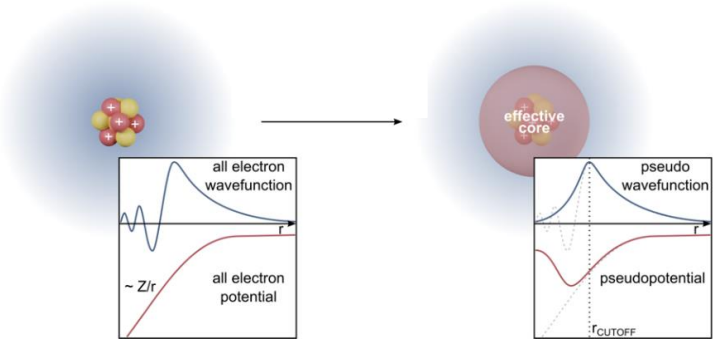

Figure 2.1. On the left the all electron potential (in red) and the all electron wavefunction (in blue) are shown. On the right the core electrons of the system are substituted by an effective core, that is realized using the pseudopotential (in red) and the pseudo wavefunction (in blue).

VASP calculations are based on the PAW (Projector-augmented wave) approach. This formalism results from a combination of Vanderbilt-type ultrasoft-pseudopotentials (USPP) and the linearized augmented-plane wave (LPAW) method [34]. In order to simplify the description of this approach a simple metallic crystal can be considered (**figure 2.2**). The system is divided in PW spheres (the metallic ions) and the space around them, that is the interstitial region. Using the pseudopotential, the problems coming from the nodes near to the nuclei disappear. The plane wave basis set can be used therefore to define the wavefunction, that is just an approximation, since it shows the good behavior in the interstitial region, but not in the PW sphere. For the latter, all electron wave functions are used. These ones are the solutions of the radial scalar relativistic Schrödinger equation for a non-spinpolarized reference atom. Combining all these information, in the PAW method the one electron wavefunction ψ_{nk} is expressed as the following linear transformation [34]:

$$|\psi_{nk}\rangle = |\tilde{\psi}_{nk}\rangle + \sum_i (|\phi_i\rangle - |\tilde{\phi}_i\rangle)\langle \tilde{p}_i|\tilde{\psi}_{nk}\rangle \qquad (\mathbf{2.4})$$

$|\tilde{\psi}_{nk}\rangle$ is the pseudo-orbital (the one derived using the pseudo-potential), expanded in plane waves. As explained above, the behavior of this function is the identical to the correct one only in the interstitial region. To take into account the correct behavior inside the spheres a second term must be included. All the functions inside the summation are atom-centered localized functions. ϕ_i is the all-electron partial wave, that is a solution of the radial non-spinpolarized Schrödinger equation. $\tilde{\phi}_i$ is the pseudized version of ϕ_i. **Figure 2.2** and **Figure 2.3** are simplified images of the PAW method.

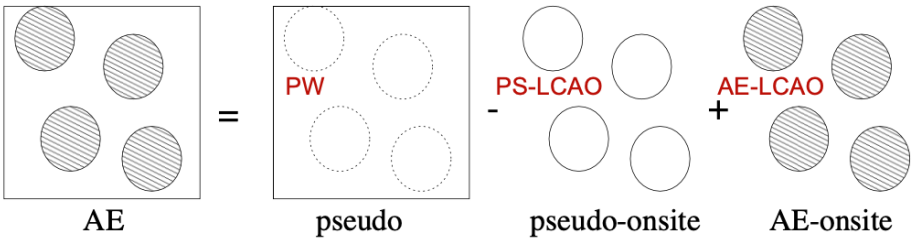

Figure 2.2. The figure shows a pictorial representation of the PAW method. The square represents the solid state system, while the circles are the constituting atoms. The entire systems, represented exactly by the all electrons wavefunction (AE) is decomposed in a particular combination of the pseudo-wavefunction, determined for the whole system using the pseudopotential (pseudo), the pseudized functions of the PW sphere (pseudo-onsite) and the functions of the PW sphere determined with the real potential of the system (AE-onsite) *[34]*.

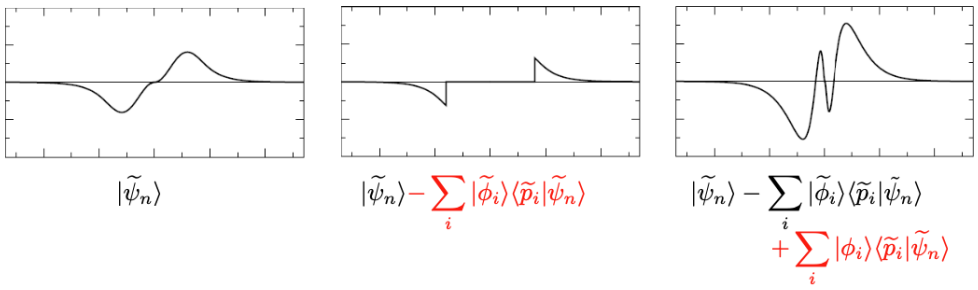

Figure 2.3. The figure shows the particular combination of wavefunctions that is used in the PAW sphere. The first image on the left is the pseudo-wavefunction. The image at the center represents the subtraction of the summation over the pseudized orbitals from the pseudo-wavefunction. The last image includes the summation over the orbitals determined with the correct potential *[34]*

VASP calculations need different input files. First of all, a POSCAR is required. This file contains mandatory the scaling factor(s), the lattice vectors, the number of ions per species and the ion positions [34]. In the POSCAR it is also possible to enable the selective dynamics, providing extra flags for each atom signaling whether its coordinate(s) are allowed to change or not during a possible ionic relaxation. Then, a POTCAR file that contains the pseudopotential for each species involved in the calculation is needed. A third input file is the KPOINTS. Since VASP is based on periodic boundary conditions, most of the central quantities are evaluated in the reciprocal space (e.g. electronic density). The KPOINTS file specifies the Bloch vectors (k points) used to sample the first Brillouin zone [34]. Different type of meshes can be used: explicit k-point mesh, regular k-point mesh, automatic k-point mesh. For the latter it is possible to choose between Γ-centered or Monkhorst-Pack. In both cases, it is necessary to specify the number of k-points for each direction. As a rule of thumb, the bigger the system, the fewer are the number of k-points needed to reach reliable results. A third input file is the INCAR. Basically, it determines "what to do and how to do it" [34].Different tags can be specified, and each of them is followed by a value (tag = value). The tags and the associated values select the algorithms and set the parameters that VASP uses during the calculations. For some tags, if the values are not explicitly indicated by the user, the code uses reasonable default values [34].

2.1.2 Ionic relaxation with VASP

Among the standard VASP calculations there is the ionic relaxation. In this type of calculation the atoms of the system are displaced in a way that they can reach a geometry with some requested characteristics, usually a minimum on the energy surface. In order to run an ionic relaxation, an appropriate INCAR file must be prepared. The crucial tag in this case is the IBRION, that determines how the ions are updated and moved [34]. For IBRION = 1, a Quasi-Newton algorithm is used to relax the ions into a point of the energy surface whose gradient is zero (i.e. a minimum, a maximum or a saddle point) [34]. It relies on an approximation of the Hessian Matrix, using the DIIS (direct inversion in the iterative subspace) algorithm. IBRION = 1 is a good choice when the starting system is close to a local minimum, otherwise it can fail badly. In the latter case, IBRION = 2 is preferable, since it relies on a conjugate gradient algorithm [34]. In both cases the termination of the calculation is set using EDIFFG tag. It is also possible to define a maximum number of iterations using the NSW tag. If the EDIFFG is reached the calculation ends, otherwise it will end when the NSW value is reached. IBRION can also have other values (e.g. 5 or 6 for the evaluation of the second order derivatives of the total energy with respect to the position of the ions) [34].

2.1.3 Transition state search with VASP

Transition states (TS) are special points of the potential energy surface. Numerically they correspond to first order saddle points, that are points where the gradient of the energy equals zero and the hessian matrix has a unique negative eigenvalue. In VASP there are three main approaches that can be used (alone or in combination) for a TS search. A first possible method is the one that starts from a reasonable guess of the transition state (e.g. known from other similar reactions previously studied). This is the simplest approach, that uses IBRION = 1. As explained in the previous section, this tag indicates a Quasi-Newton algorithm that allows to find points where the gradient is zero (i.e. a minimum, a maximum or a saddle point) [34]. Starting from a reasonable guess, hopefully, the system will evolve to the nearest stationary point, that is the transition state. The frequencies of the normal modes of vibration of the system can be calculated (i.e. IBRION = 5) [34]. If there is just one imaginary frequency the point is a firs order saddle point. Quite often, the system is far away from the transition state and it is more probable that it will end in a local minimum instead of a saddle point. The other two methods for the TS search are based on a search along a path that connects two minima previously found. From a chemical point of view the transition state corresponds, in fact, to the

highest energy point along the reaction coordinate, that is the special path connecting the reactants and the products. Once the two minima are known, some other geometries along a non-optimal path, that connects them must be generated. In this work the Opt'n Path program, by Paul Fleurat-Lessard is used [37]. It is based on a mixed systems of coordinates (cartesian for the frozen atoms, internal for the others) [37]. After the generation of the path, the NEB (Nudged Elastic Band) method or the DIMER method can be used. The former requires an optimization of the images previously generated, in order to find an optimal path or a proper guess for the next step of the TS search (**Figure 2.4**). If a standard optimization of the images would be done, they will quite surely end in the nearest minimum (i.e. the reactant or the product), making the optimization useless. The solution is to apply a potential constrain between the images (i.e. the "spring"), in order to optimize them without reaching the reactant or the product [38].

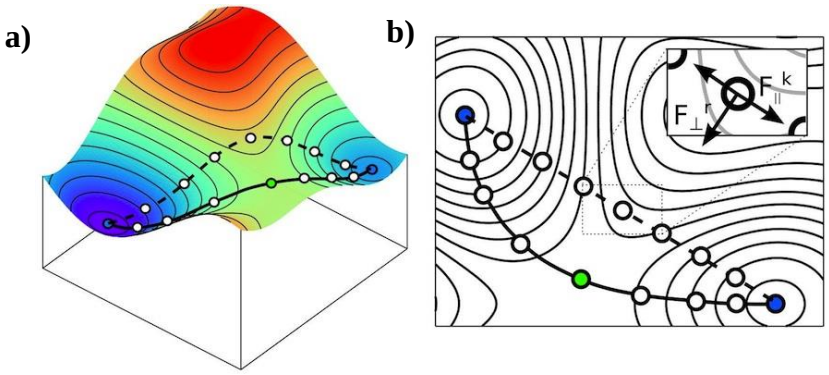

Figure 2.4. (a) The energy surface is represented. The dotted path that connects the two minima (blue points) is a non-optimal one. The continuous line path, instead, is the optimized version and the green point represents the transition state. **(b)** The level curves representations of the same path are shown. The blue points are the minima, while the green one is the TS . (https://umet.univ-lille.fr/Projets/RheoMan/en/to-learn-more-about/nudged-elastic-band.php.html)

The images higher in energy are the ones that are supposed to be closer to the TS. These points can be characterized, and if among them there is no saddle point, other search strategies can be used to reach the TS.

Another possible approach is the DIMER method. In this case some informations are added to orient the search. A new input file, called MODECAR is required. It contains the vector that indicates the direction along which the optimization should be performed [39]. The vector of one imaginary normal mode, for a structure of the reaction path, can be used (i.e. the one whose vibrations are along the reasonable reaction path).

2.2 Computational Hydrogen Electrode (CHE)

Computational Hydrogen Electrode (CHE) is one of the most used approaches in the field of atomistic modeling for electrocatalysis. This method takes into account the influence of an applied electrode potential on the energy profile of a reaction in a straightforward manner. The effect of the electrode potential is not included inside the QM calculation, but it is introduced a posteriori, with the chemical potential of the couple ($H^+ + e^-$) expressed as a function of it [25].

In the case of an electrocatalyzed reaction a reaction network needs to be defined and investigated, that means that a certain number of reactive steps must be considered. These ones can be divided into electrochemical and "chemical" (i.e. steps where an electron transfer is involved or not). The energetic of both the type of steps is influenced by the electrode potential. For the former it is simpler to understand, since they happen with an electron transfer, for the latter, changing the electrode potential, the interaction between a charged surface and a molecule adsorbed on it can change, and then the adsorption mode and the energy of adsorption can also change. The CHE method is not able to take into account the influence of the electrode potential on the "chemical" steps, since the effect of the potential is evaluated only on the energy of the couple ($H^+ + e^-$) , that, as a definition, is not involved in "chemical" steps. Furthermore, the effect of the electrode potential cannot be considered for all the types of electrochemical steps, but only where a proton coupled electron transfer (PCET) is involved. This is a strong limitation, since in the lest years more and more experimental evidences are emerging about the key role of decoupled pathways [26]. Another drawback of the CHE is that it only allows the evaluation of the thermodynamics of the elementary reaction steps [26]. The activation barrier for the electrochemical steps is usually ignored, even though some approaches have been developed to approximate the potential dependence of barriers [21]. Finally, another strong approximation of the method is the negligibility of the solvation effects. Actually, some authors use the CHE in conjunction with solvation effects [26]. It is important to consider that the presence of a charged surface has an influence also on the solvents. CHE is unable to deal with this effect, since an explicit charged surface is absent in the QM calculation.

The first step in the application of the CHE method is the evaluation of the chemical potential for the couple ($H^+ + e^-$). This quantity is not determined by an ab-initio computation, but in a straightforward manner, that is one of the reasons behind the great diffusion of the method. J. Nørskov and his collaborators, observed that, defining 0 V of the standard hydrogen electrode

(SHE), under standard conditions (pH = 0, T = 298 K, p = 1bar), there is an equilibrium between hydrogen molecules in the gas phase and solvated protons and electrons [25]:

$$\frac{1}{2}H_{2\,(g)} \rightleftarrows H^+ + e^- \qquad (\mathbf{2.5})$$

Since the reaction is at the equilibrium, $\Delta G = 0$:

$$\mu_{H^+}(U = 0\ vs\ SHE) + \mu_{e^-}(U = 0\ vs\ SHE) - \frac{1}{2}\,G_{H_2} = 0 \qquad (\mathbf{2.6})$$

$$\mu_{H^+}(U = 0\ vs\ SHE) + \mu_{e^-}(U = 0\ vs\ SHE) = \frac{1}{2}\,G_{H_2} \qquad (\mathbf{2.7})$$

Once the free energy of the H_2 in the gas phase is calculated, dividing it by a two factor the chemical potential of the couple (H^+ + e^-) is available (**Equation 2.7**). The ab initio computation of a complicated quantity ($\mu_{H^+} + \mu_{e^-}$), is substituted by the ab initio computation of a really simple one (G_{H_2}). The electrochemical potential of (H^+ + e^-) is defined as:

$$\mu_{H^+}(U\ vs\ SHE) + \mu_{e^-}(U\ vs\ SHE) = \mu_{H^+}(U = 0\ vs\ SHE) + \mu_{e^-}(U = 0\ vs\ SHE) - neU - k_bTpHln(10) \qquad (\mathbf{2.8})$$

Where n is the number of electrons involved in a reactive step, U is the electrode potential, T is the temperature and pH is the pH of the solution. Substituting the **Equation 2.7** in the **Equation 2.8**:

$$\mu_{H^+}(U\ vs\ SHE) + \mu_{e^-}(U\ vs\ SHE) = \frac{1}{2}\,G_{H_2} - neU - k_bTpHln(10) \qquad (\mathbf{2.9})$$

Equation 2.9 defines the expression commonly used to define how the electrochemical potential of (H^+ + e^-) depends on the electrode potential [26].

Once the hypothetical reaction network of an electrocatalyzed reaction is defined, the reaction energy for each step can be evaluated. The free energies of the reactants and of the products are calculated with a QM method (e.g. using DFT method implemented in VASP). The reaction free energy can be then evaluated as:

$$\Delta G = G_{products} - G_{reactants} \qquad (\mathbf{2.10})$$

Among the reaction steps that are also the ones involving a proton coupled electron transfer. In this case, also the chemical potential of $(H^+ + e^-)$ must be included in the expression of ΔG, exactly as every other reactant or product. As an example consider a reduction half-reaction:

$$Ox + H^+ + e^- \rightarrow Red \qquad (\mathbf{2.11})$$

In this case:

$$\Delta G = G_{red} - G_{ox} - (\mu_{H^+}(U\ vs\ SHE) + \mu_{e^-}(U\ vs\ SHE)) \qquad (\mathbf{2.12})$$

$$\Delta G = G_{red} - G_{ox} - (\frac{1}{2} G_{H_2} - neU - k_b TpHln(10)) \qquad (\mathbf{2.13})$$

Equation 2.13 shows as, for this type of steps, the energy can be expressed as a function of the electrode potential (U). Changing U the energy of these steps will change. For all the other types of steps the thermodynamic is not influenced by the application of the electrode potential, in the context of the CHE.

2.3 Grand-Canonical density functional theory (GC-DFT)

GC-DFT (Grand Canonical Density Functional Theory) is one of the approaches that allows to go beyond the CHE approximation. This method is able to face the two major drawbacks of the CHE, that are also the two major challenges in the accurate description of electrochemical phenomena: the presence of the solvent/electrolyte and the presence of an explicit charged surface [27].

VASPsol package developed by K. Mathew and his collaborators [31] [30] describes the solute explicitly using DFT, while the electrolyte is described using the linearized Poisson-Boltzmann equation [31]. The most crucial aspect is the ability of the method to describe the interface, where an electrostatic coupling of the DFT and Poisson-Boltzmann equation is required. Following the JDFT theoretical approach, the total free energy can be defined as a functional of both the solute electronic charge density ($n(\vec{r})$) and the net electrostatic potential of the system ($\phi(\vec{r})$) [31]:

$$A\,[n(\vec{r}),\phi(\vec{r})] = A_{TXC}[n(\vec{r})] + \int \phi(\vec{r})\rho_s(\vec{r})d^3r - \int \varepsilon(\vec{r})\frac{|\nabla\phi|^2}{8\pi}d^3r + \int \frac{1}{2}\phi(\vec{r})\rho_{ion}d^3r + A_{cav} + A_{ion} \quad (\mathbf{2.14})$$

In expression 2.14, the first term on the right is the free energy density functional describing the kinetic and exchange-correlation energy of the solute. The following three terms comes from the electrostatic interactions between the charge densities and system's electrostatic potential, where $\rho_s(\vec{r})$ is the total solute charge density, expressed as the sum of electronic and nuclear charge densities; $\rho_{ion}(\vec{r})$, instead is the ion charge density of the electrolyte, defined as [31]:

$$\rho_{ion}(\vec{r}) = \sum_i qz_i c_i(\vec{r}) \quad (\mathbf{2.15})$$

The term inside the summation is a product of the elementary charge, the formal charge of the ion and its concentration. That is expected to change moving from the bulk (${c_i}^0$) to the charged surface. This change is given by a multiplication between ${c_i}^0$, the shape function ($\zeta[n(\vec{r})]$) and a Boltzmann factor of the electrostatic energy [31]:

$$c_i(\vec{r}) = \zeta[n(\vec{r})]{c_i}^0 exp\left(\frac{-z_i q\phi(\vec{r})}{k_b T}\right) \quad (\mathbf{2.16})$$

where the shape function $\zeta[n(\vec{r})]$ is defined as [30]:

$$\zeta[n(\vec{r})] = \frac{1}{2}erfc\left\{\frac{log(n/n_c)}{\sigma\sqrt{2}}\right\} \quad (\mathbf{2.17})$$

It is used in order to scale the electrolyte properties when moving from the bulk to the interface (**Figure 2.5**). Among the implicit solvent properties that change near the surface, there is mostly the relative permittivity of the electrolyte. This quantity is expressed as a local function of the electronic charge density of the solute, modulated by the shape function [31]:

$$\epsilon(n(\vec{r})) = 1 + (\epsilon_b - 1)\zeta(n(\vec{r})) \quad (\mathbf{2.18})$$

The last two terms in expression 2.14 are some of the non-electrostatic interactions. A_{cav} describes the free energy contributions of cavitation, dispersion and the repulsion interactions between the solute and the solvent. This term is defined to be a function of the surface tension parameter τ and the solvent-accessible area (i.e. the shape function) [30]:

$$A_{cav} = \tau \int |\nabla \zeta[n(\vec{r})]| \, d^3r \qquad (\mathbf{2.19})$$

Finally, A_{ion} is the non-electrostatic contribution from the mobile ions in the electrolyte. It can be assumed that this contribution comes mainly from the entropy term [31]:

$$A_{ion} = k_b T S_{ion} \qquad (\mathbf{2.20})$$

The most interesting points of the free energy surface are the stationary ones. In order to find them. the first order derivative with respect to the electronic charge density of the solute $n(\vec{r})$ and the system potential $\phi(\vec{r})$, can be evaluated and set to zero. The first minimization leads to the typical Kohn Sham Hamiltonian, where an additional term is present in the local part of the potential, corresponding to all the terms that account for the presence of the solvent/electrolyte [31]. The second minimization yields to the generalize Poisson-Boltzmann equation [31]:

$$\vec{\nabla} \cdot \epsilon \vec{\nabla} \phi = -\rho_s - \rho_{ion} \qquad (\mathbf{2.21})$$

Assuming that electrolytes with only two types of ions are present, with charge equal and opposite and with the same concentration in the bulk, the above expression becomes [31]:

$$\vec{\nabla} \cdot \epsilon \vec{\nabla} \phi = -\rho_s + 2\zeta[n(\vec{r})] qzc^0 sinh\left(\frac{zq\phi}{k_B T}\right) \qquad (\mathbf{2.22})$$

If the argument of the hyperbolic sine is much smaller than 1, the expression 2.22 can be further simplified into the linear Poisson-Boltzmann equation, that is the one used in VASPsol [31]:

$$\vec{\nabla} \cdot \epsilon \vec{\nabla} \phi - \kappa^2 \phi = -\rho_s \qquad (\mathbf{2.23})$$

In order to evaluate the energy of the solvated system the solutions of the modified Kohn Sham equations and the linearized Poisson-Boltzmann equation must be coupled. In fact, the

additional term in the Kohn Sham functional, that accounts for the presence of the solvent/electrolyte, depends on the electrostatic potential ϕ, that is a solution of the Poisson Boltzmann equation. At the same time the Poisson-Boltzmann equation contains the permittivity ϵ that changes as a function of the solute electronic density (**Equation 2.18**) that is a quantity coming from the solutions of the Kohn Sham equations. Coupling the two equations the interface between the solute and the solvent/electrolyte is finally described, in the limit of all the approximations introduced.

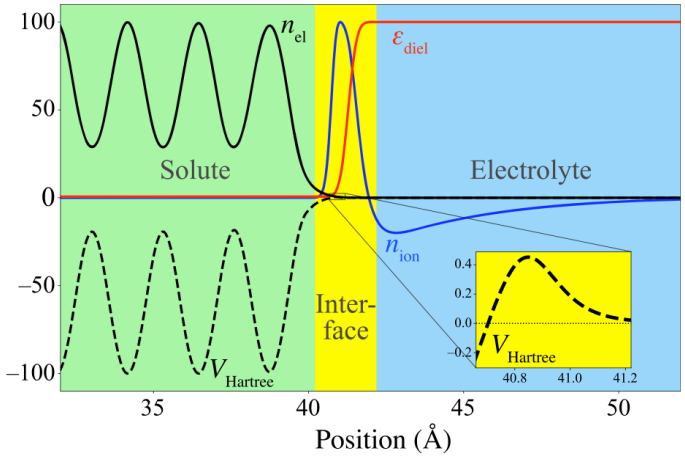

Figure 2.5. The potential (V), the dielectric constant (ε) *and* the ion density (η_{ion}) are represented as a function of the distance from the charged surface. The properties are shown as a percentage of their maximum value. The system is divided in: solute (in green), interface (in yellow) and electrolyte (in blue) [31].

Once the presence of the solvent/electrolyte is considered, the second major challenge must be faced. Experimental measures in electrocatalysis are quite often done in potentiostatic conditions, that means with a constant electrode potential. For this reasons information about the energetic of the systems at different electrostatic potential are needed. One of the possible approaches, that is also the same used in this work, is to change the number of electrons of the system and redo the calculation. The major drawback of this approach is that a countercharge is needed in order to make the cell neutral, otherwise the energy would go to infinity. Using the VASPsol implicit model the problem is solved in an elegant and easy way, since the linearized Poisson-Boltzmann equation automatically generates neutral unit cells [26]. A technical issue is the need to create a symmetric system in order to delete the dipole vectors, that can create concern during the calculation. The energy of the system can be transformed in the grand-canonical energy, F (since the systems we are studying is, in fact, a grand canonical

ensemble), that is the Legendre Transformation of the free energy [31] [40]. The dependence of this quantity from the potential can be approximated as:

$$F(U) = E(U) - q(U) \cdot U \approx E(U_0) - \frac{1}{2} C(U - U_0) \qquad (\mathbf{2.24})$$

where a quadratic dependence on the electrochemical potential U appears [26]. Grand-canonical energies against the corresponding electrochemical potentials can be fitted, obtaining parabolas (**Figure 2.6**). Once the fitting is done, the energies are finally expressed as functions of the electrochemical potential at a moderate computational cost [26].

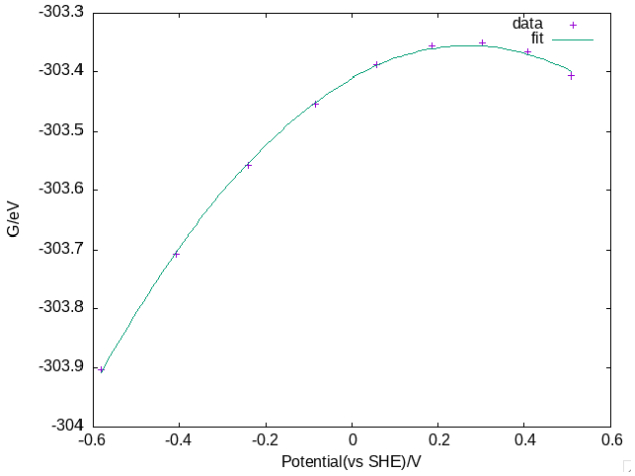

Figure 2.6. The energy G as a function of the Potential vs SHE for a Cu p(4X4) 5L symmetric slab. Data are fitted with a parabolic function.

3 Computational details

3.1 VASP

In order to build the energy profiles for the reaction network, DFT calculations must be performed. Since in heterogeneous electrocatalysis, reactions take place on solid surfaces, a periodic code is needed. The main computational tool in this work is VASP. In particular, the version VASP 6.2.1 was used. In the context of GC-DFT the VASPsol package was exploited to simulate the electrode/electrolyte interface. In the following subchapters the major features of the input files used for this work are described.

3.1.1 POSCAR

The POSCAR files collect the spatial coordinates of the system. Experimental catalysts characterizations show that (111) facet is the one more likely to be exposed by Ag; for Cu, instead there are not preferential facets. For these reasons, (111) facet for both the metals has been considered in this study. The lattice parameters for Ag and Cu, were evaluated through bulk calculations in VASP. The electrode surface has been modeled as a p(4x4) supercell before and as a p(6x6) supercell, with five layers (5L) and 19 Å of vacuum in both cases. These features are a good compromise to shorten calculations and at the same time to avoid strong interactions between the molecule adsorbed on one slab and its periodic images. Since the presence of the dipole can create drawbacks in the calculations, it is canceled using a symmetrical system. A point symmetry, whose center is a point of the third layer of the slab, is used. In case of adsorbed molecules two symmetric molecules are therefore present, one on the first layer and another one on the fifth layer (**Figure 3.1**). The software Avogadro has been used to build the POSCAR in case of molecules adsorbed on the metal slabs, and a python script was exploited to build the symmetric system. Selective dynamics has been enabled for all the optimization calculations. The central layer is maintained frozen (F F F), all the others and the coordinates of the molecule adsorbed too are allowed to change in all space directions (T T T).

3.1.2 KPOINTS

The automatic mesh has been enabled. In particular, a $5 \times 5 \times 1$ gamma centered mesh has been used for the p(4x4) supercell, while for the p(6x6) a $1 \times 1 \times 1$ gamma centered mesh has been exploited. Tests on the system showed that these are the best compromise between accuracy and time of calculation, in each case.

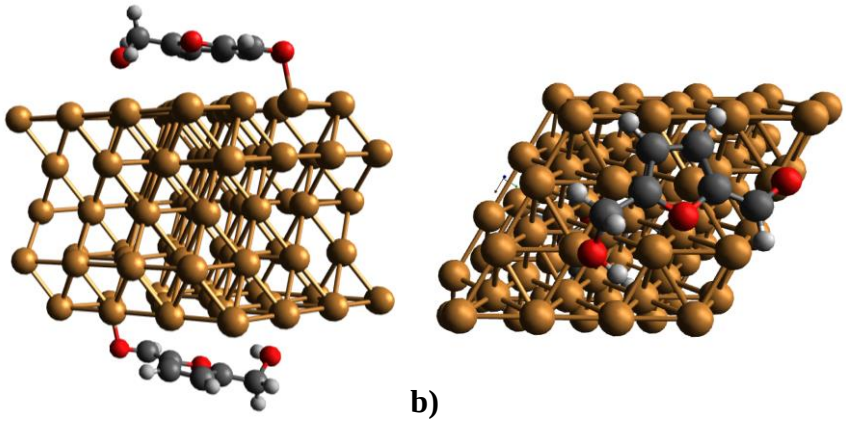

Figure 3.1. The symmetrized structure of HMF adsorbed over Cu(111) 4x4 supercell is shown with **(a)** a lateral view and **(b)** a top view.

3.1.3 INCAR

The tags and their related values depend on the type of calculation that is performed.

In the case of geometrical optimization for the adsorbed chemical species, the following INCAR has been used:

PREC = Normal
EDIFF = 1e-6
GGA = PE
IVDW = 4
ALGO = Fast
LREAL = Auto
ENCUT = 400
ENAUG = 844.9
NSW = 300
IBRION = 2
POTIM = 0.5
EDIFFG = -0.02
ISMEAR = 2

Most of the tag values used in the INCAR were chosen because of the experience with similar systems. The conjugate gradient algorithm (IBRION = 2) was exploited for all the geometrical optimizations. The functional used is the PBE (Perdew-Burke-Ernzerhof), a GGA (generalized gradient approximation) functional, with usually a reasonable accuracy [41]. To consider the non electrostatic interactions, dDsC dispersion correction developed by S. N. Steinmann and C. Corminboeuf has been used (IVDW = 4) [42] [43].

In the case of GC-DFT calculations, also the existence of a solid/electrolyte interface needs to be considered. Calculations are performed using VASPsol package; some tags are added:

LSOL = .TRUE.
TAU = 0.00
LAMBDA_D_K = 3.0
NC_K = 0.0025 or 0.00025

The first tag enables the presence of the solvent. By default, water is considered, otherwise the dielectric constant of the medium must be added to the INCAR. The second tag refers to the cavity tension. The third is the Debye Length of the electrolyte, whose value has been chosen using the experience on similar system. The last tag refers to the "distance" of the solvent from the system; in practice, the higher is the value, the closer it is. This value is crucial since no explicit molecules of the solvent are present. If the solvent is too far, the system is not well solvated; if it is too close it can go inside the metal slab or between the molecule and the surface, creating unphysical situations. Some tests were performed on HMF adsorbed over Cu(111) slab (4x4 supercell) in order to find the best value for the tag. For both the values tested (0.0025 and 0.00025) the adsorption energy becomes more positive, increasing the electrode potential. In the case of 0.00025 energies are more negative than 0.0025, suggesting a less solvated system. The solvent density (RHOB and RHOION files) for both the cases was visualized using VMD, showing no unphysical situations (**figure 3.2**). This evidence suggested the use of NC_K = 0.0025.

a) **b)**

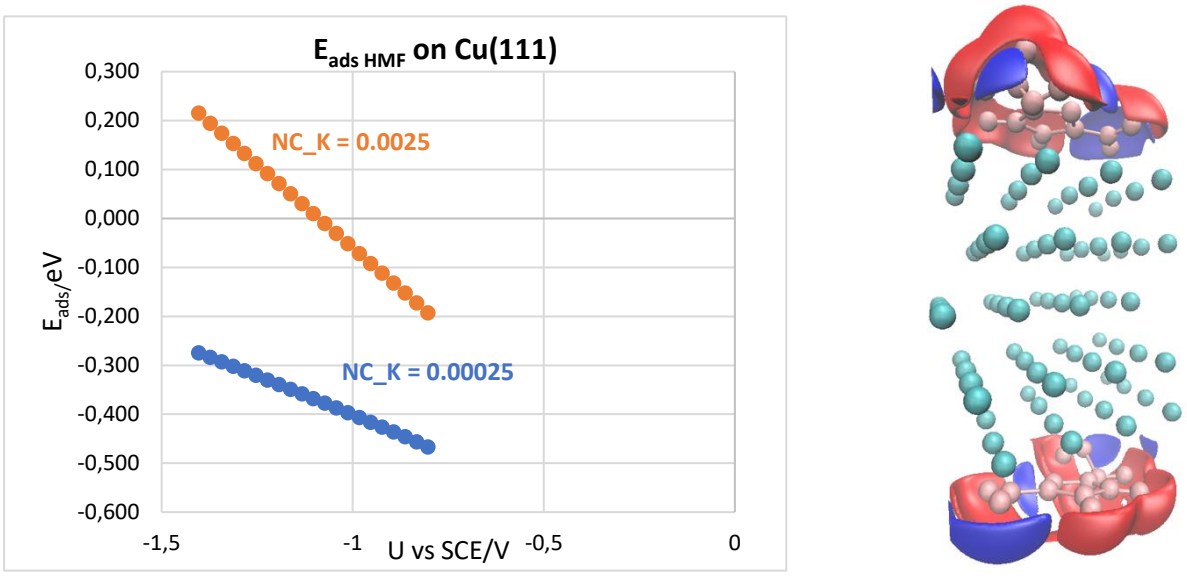

Figure 3.2. In graph **(a)** The potential adsorption energy (no entropy contributions) for HMF over Cu(111) 4x4 supercell and 5 layers is plotted against the electrode potential, for two NC_K values. The orange dots refer to NC_K = 0.0025 while the blue ones refer to NC_K = 0.00025. (**b)** The solvent density, for HMF adsorbed on Cu(111) with a charge of +0.75 (NC_K = 0.0025). The density is represented using isosurfaces (red refers to positive density with isovalue of 0.000847, while blu refers to negative density with isovalue of -0.000872). Pink spheres represent HMF atoms, while the azure ones are the Cu atoms of the slab.

3.2 Energy profiles computation

Once VASP ionic relaxation for each intermediate ends, its energy is extracted from the OUTCAR file. This value is the potential electronic energy (E_{el}). To figure out if a reaction, held at constant pressure and temperature, is spontaneous or not, the difference in Gibbs free energy (G) is required. The reaction energy profiles are, therefore, built plotting the Gibbs free energy of each species involved in the reactive steps, referred to HMF molecule and the metal slab at infinite distance, against the reaction coordinate. Activation barriers are ignored in this study. The reaction coordinate chosen is the number of (H^+ + e^-) couples that must be transferred till the formation of the specific chemical specie, as it is commonly done in literature.

To plot the reaction energy profiles, Gibbs free energy must be computed. This quantity is defined as:

$$G = H - TS \qquad (3.1)$$

Where H is the enthalpy, T is the temperature and S is the entropy. For each species, the entropy in **Equation 3.1** can be decomposed in different terms:

$$G = H - T(S_{trans} + S_{rot} + S_{vib} + S_{el} + S_{conf}) \quad (\mathbf{3.2})$$

namely: translational, rotational, vibrational, electronic and configurational entropy.
At constant temperature and pressure (i.e. typical reaction conditions), the Gibbs free energy difference for a reaction step is defined as:

$$\Delta G = \Delta H - T\Delta S \quad (\mathbf{3.3})$$

$$\Delta G = \Delta H - T(\Delta S_{trans} + \Delta S_{rot} + \Delta S_{vib} + \Delta S_{el} + \Delta S_{conf}) \quad (\mathbf{3.4})$$

Usually, the last two terms in **Equation 3.2** can be approximated to zero. The first two terms, instead, could be crucial or not. In the case of adsorbed molecules they are zero, since translational and rotational degrees of freedom are absent. Instead for desorbed molecules they must be taken into account. The easiest approach is to treat the molecule as a perfect gas and a perfect rotator. In these cases exact equations have been developed in statistical mechanics. In this work the IdealGasThermo module of the ASE (Atomic Simulation Environment) has been used to evaluate S_{trans} and S_{rot}. Vibrational term, instead, is an important contribution for both, desorbed molecules, and adsorbed ones. It can be computed modeling the system as a harmonic oscillator, using the equations of statistical mechanics. Although it won't require too much time for the desorbed species, a greater effort is required for adsorbed ones, where the molecule and the slab together must be considered . In this work it is assumed that the vibrational contributions are similar between different species involved, and for this reason the ΔS_{vib} in equation 3.4 is always approximated to zero. Intuitively this approximation could be really bad for adsorption/desorption reactions.
Finally, G can be computed. Two different expressions are used for the adsorbed species (**Equation 3.5**) and the desorbed ones (**Equation 3.6**):

$$G \approx H - TS_{vib} \quad (\mathbf{3.5})$$

$$G \approx H - T(S_{trans} + S_{rot} + S_{vib}) \quad (\mathbf{3.6})$$

In the case of the desorbed species, if the species are in gas phase, as in the case of CHE approach, S_{trans} and S_{rot} terms are the ones coming from ideal gas approximation. If the species are solvated, like in the GC-DFT framework, the degrees of freedom are reduced and S_{trans} and S_{rot} are corrected:

$$G \approx H - 0{,}54 \times T(S_{trans} + S_{rot} + S_{vib}) - 2{,}86 \times 10^{-4}T \qquad (\mathbf{3.7})$$

Finally, the difference in free energy for each step is computed as:

$$\Delta G = \Delta H - T\Delta S \approx \Delta E_{el} - T(\Delta S_{trans} + \Delta S_{rot}) \qquad (\mathbf{3.8})$$

4 Results and discussion

4.1 Reaction Network

This work aims to explain the different performances of Cu/Cu foam and Ag/Ag foam catalysts for HMF electrocatalytic hydrogenation (ECH) in a basic medium, through an atomic scale insight. Elucidations on the reaction mechanism for both the metallic surfaces therefore are needed. The first step of this study is the definition of a hypothetical reaction network for HMF electrocatalytic hydrogenation. Literature search and supporting experimental evidences have been exploited to build the network under investigation in this study (**Figure 4.1**) [10] [17] [5] [44] [45]. In the reaction network only PCET mechanism is investigated, since there are no evidences that suggest HAT as the predominant one. For PCET, the electrochemical steps always include the transfer of the ($H^+ + e^-$) couple, which allows the use of the CHE theoretical framework, as a first approximation. A refinement with GC-DFT is done subsequently.

Data in literature showed the formation of BHMF, MF, MFA, DMF and BHH, when the reaction is performed in a basic medium [1] [45]. BHMF is the product of interest, for which the highest selectivity, productivity and faradaic efficiency are desired. It is formed through the hydrogenation of the aldehyde group of the reactant. MF is a crucial side product since it is an intermediate in MFA and DMF production [45], which is formed through the hydrogenolysis of the C-OH bond of HMF. MFA is a side product, characterized by the presence of a methyl group that is formed through the hydrogenolysis of the aldehyde group of HMF. Finally, the BHH dimer comes from the electrocatalytic dimerization of HMF. Many studies suggest that not only dimer, but also humines could be formed under electrocatalytic reduction of HMF [17] [1] [16], but their structure has not been characterized in literature. Among possible products there is also the DMF, that is a furanic ring with two methyl groups, which is formed through the hydrogenolysis of both the C=O and the C-OH groups of HMF.

A route for each product has been defined in the reaction network. In **Figure 4.1** the green arrows refer to the paths toward BHMF, the yellow ones toward MF, the pink ones towards MFA, the brown ones toward DMF and finally the red ones toward BHH. It is supposed that further oligomerization (i.e. humines formation) start from BHH.

The route to BHMF involves two possible intermediates: **I01***, an alkoxy radical formed after the PCET on the carbon of C=O, and **I02***, an hydroxyalkyl radical formed from the PCET on the oxygen of C=O. Subsequent PCET forms BHMF, from both the intermediates. The intermediate **I02*** can be involved in a pinacol coupling over the surface with another **I02***, forming BHH, which is supposed to undergo further oligomerization or polymerization.

Instead of a PCET transfer, the adsorption of HMF can be followed by a fragmentation of the C-OH bond yielding to **I06*** and **OH***. **I06*** can be involved in a subsequent PCET, generating MF. The MFA, instead, can be formed in several ways: from MF, from **I01***, from **I02*** or from BHMF, always through a C-O bond fragmentation, followed by different PCETs. Finally, DMF can be generated from MF or MFA.

Beyond the reactions involving HMF also the HER should be considered. The first step of HER is the Volmer step, in which an adsorbed hydrogen (H*) is formed. It can be followed by Tafel and Heyrovsky steps that lead to the formation of H_2, a side product. Therefore, HER can impact on the faradaic efficiency. Moreover, if the HAT mechanism is the predominant one, Volmer step is shared between HER and HMF-ECH, meaning that a competition between the two reactions is observed also for the reactant (H*) and not only electron transfer. For this reason, this work also includes the study of the hydrogen coverage for both Cu(111) and Ag(111) as a function of the potential.

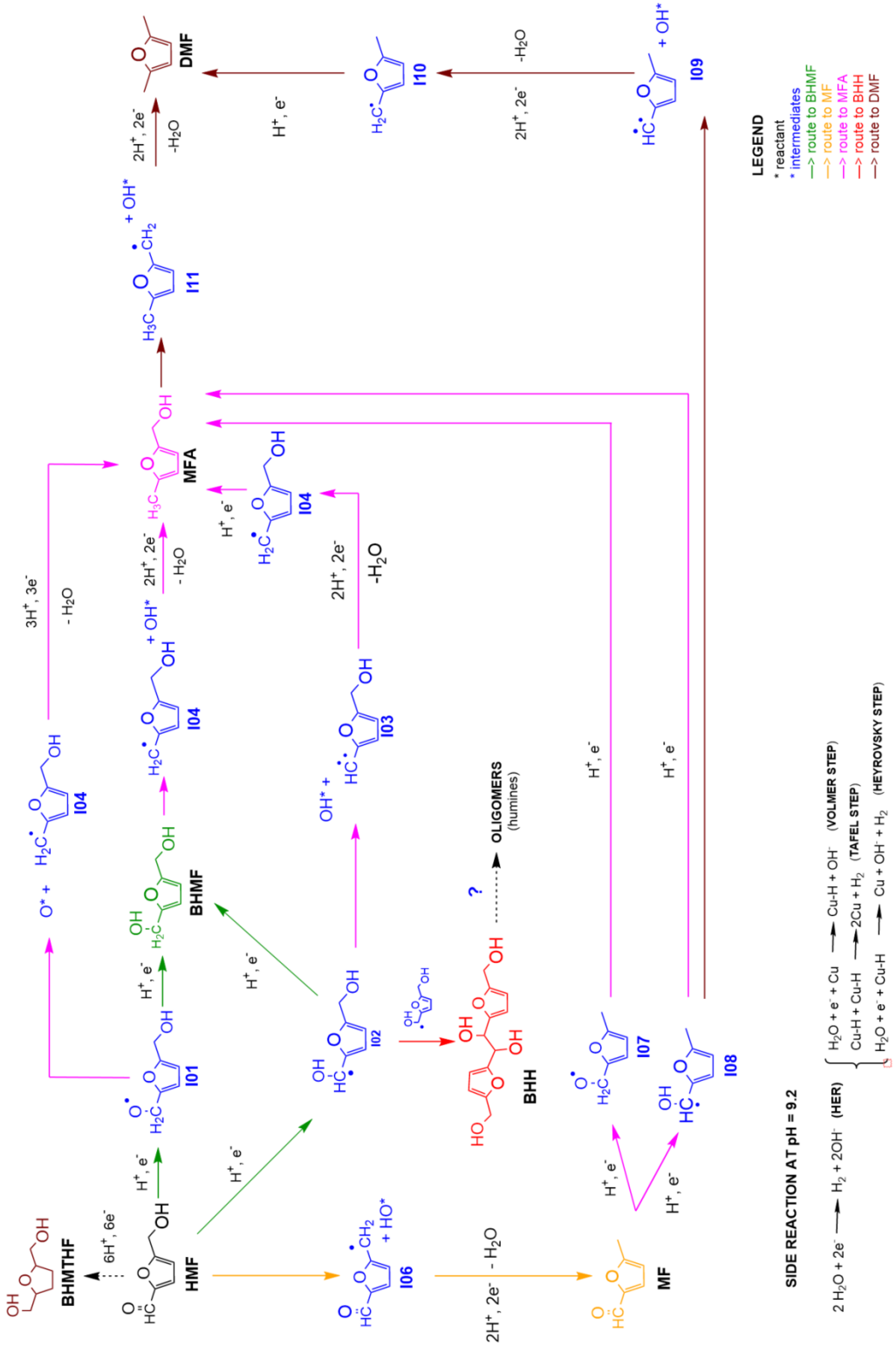

Figure 4.1. Reaction network for HMF electrocatalytic reduction. Only PCET steps are considered. The green arrows show the routes to BHMF (the desired product), while the yellow, pink, brown and red lead to side products (namely MF, MFA, DMF, BHH, respectively). The radical intermediates are shown in blue. The products instead are represented with the same color of the arrows that lead to their formation and their acronym is bolded. Below, also the steps of the competing HER are shown.

4.2 Adsorption energies

Before moving to electrochemistry, it is worth focusing on the adsorption modes and energies of the compounds involved in the reaction network, shedding light in the difference between Cu(111) and Ag(111).

Considering the symmetrized systems, the adsorption process of the X molecule over the metal surface M can be written as:

$$2\,X + M \rightarrow MX_2 \qquad (\mathbf{4.1})$$

Adsorption energy is computed as:

$$\Delta E_{ads} = 0.5 \times (E_{MX_2} - E_M - 2E_X) \qquad (\mathbf{4.2})$$

Where E is the VASP output energy. The solvent is ignored.

Different adsorption modes for each species have been investigated in the case of Cu(111) and Ag(111), aiming to find the most stable ones. To reduce the number of possibilities, preliminary calculations have been performed for model molecules, which possess separately the functional groups of HMF. In particular, the adsorption of furan, ethanol and ethanal have been investigated for Cu(111). The furan prefers a flat adsorption mode, while the alcoholic group of ethanol prefers an adsorption on *top* of Cu atoms. The carbonyl group of ethanal is adsorbed with the plane of the molecule perpendicular to the metallic surface. Cumulating this information, a reduced amount of adsorption possibilities has been explored for HMF and the other intermediates of the reaction network.

In **Figure 4.2.a**, the adsorbed structures of HMF are shown. The molecule, like all its derivatives, prefers to be adsorbed with a nearly flat adsorption mode over Cu(111). In the most stable adsorption mode, HMF alcoholic function is adsorbed in *top* position and also the oxygen atom of the carbonyl is in *top* position, with an adsorption energy of -0.83 eV. A little geometrical distortion is observed. The same adsorption mode has been described as the most stable one by Plucksacholatarn and coworkers, although they found a more exotermic adsorption energy (-1.23 eV) [12]. This discrepancy might be ascribed to the dispersion correction used (DFT-D3 instead of dDsC).

The adsorption mode of HMF over Ag(111) is quite similar to the one of Cu(111), but its adsorption energy is a little bit less exothermic (-0.76 eV). HMF is farther from the surface and

less distorted in the case of Ag(111) than for Cu(111). The distance between OH and the surface is 2.72 Å for Ag(111) and 2.34 Å for Cu(111). The carbonyl bond is elongated by 0.70% in the case of Ag(111), but 3.66% for Cu(111). The C-OH bond is elongated by 0.77% for both the metallic surfaces. The change of the adsorption energy is linked to the structural differences between the molecule adsorbed on Cu(111) and on Ag(111): the more the structural distortion and the proximity to the surface, the more exothermic the adsorption energy.

Other important intermediates are **I01*** and **I02***. Their adsorption modes are showed in **Figure 4.2.b** and **4.2c**. In the case of **I01***, for both the metals the OH goes on *top* of the metallic atom, the ring is nearly flat with the O radical, nearer to the surface and adsorbed on a threefold hollow site. In the case of **I02***, the C radical is adsorbed for both the metals on a *top* position. For both the intermediates the structures are closer to the surface and a bit more distorted for Cu(111) than for Ag(111)

Also, for the case of BHMF the adsorption mode between the two metals is similar, as shown in **Figure 4.2.d**. It has a flat adsorption mode, with the two OH groups almost on *top* positions. The distance of the OH group from the surface is 2.23 Å for Cu(111) and 2.55 Å for Ag(111). The two C-OH bonds are not elongated for both the metals. The adsorption energy is -1.06 eV for Cu(111), while it is -0.91 for Ag(111).

In the case of BHH, for the identification of the most interesting adsorption mode, different diastereoisomers have been studied. Once the most stable one has been identified, different adsorption modes have been investigated. The most stable adsorption mode of BHH is quite similar for Ag(111) and Cu(111). In both cases, one of the furanic ring has a nearly flat adsorption, while the other one is nearly perpendicular to the surface (**Figure 4.5.e**). In this way the interaction of the alcoholic function of the molecule with the surface is maximized. A similar adsorption energy is observed over Cu(111) and Ag(111).

a)

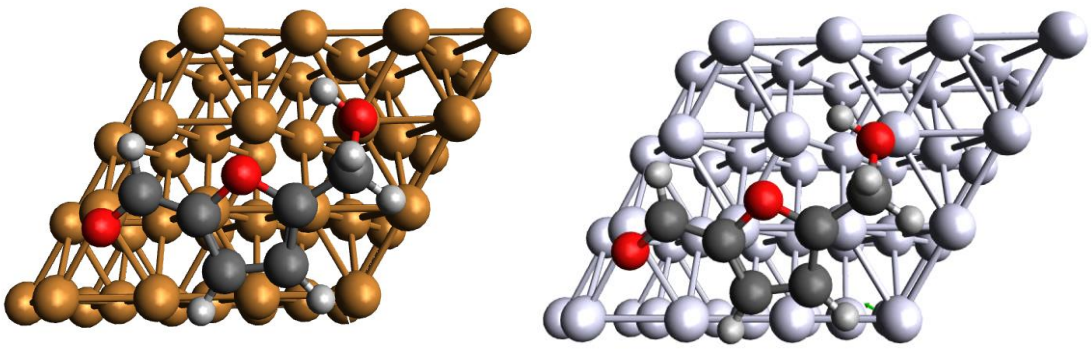

HMF

b)

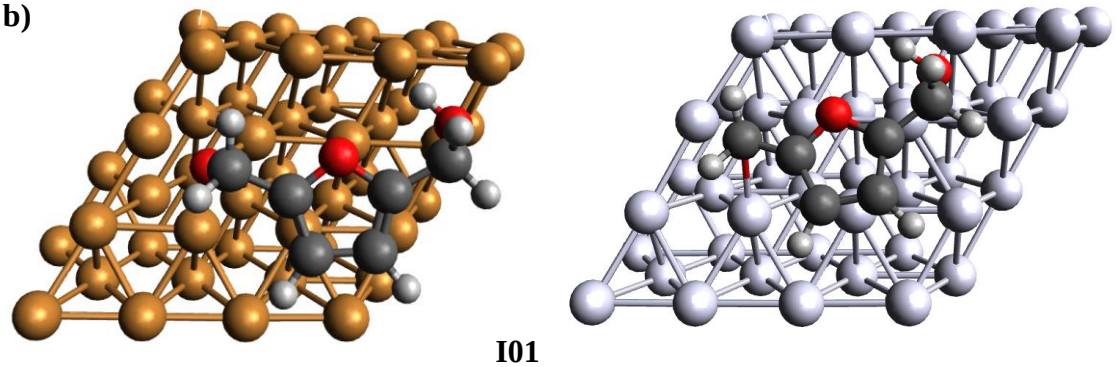

I01

c)

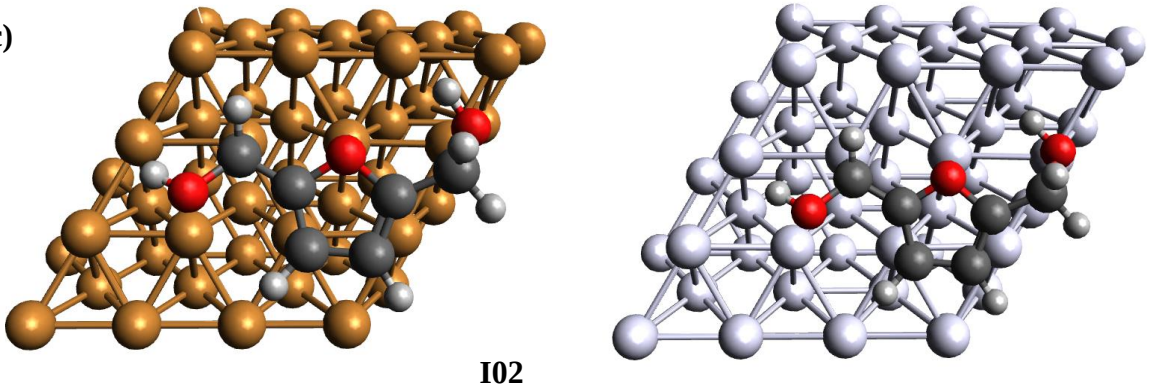

I02

d)

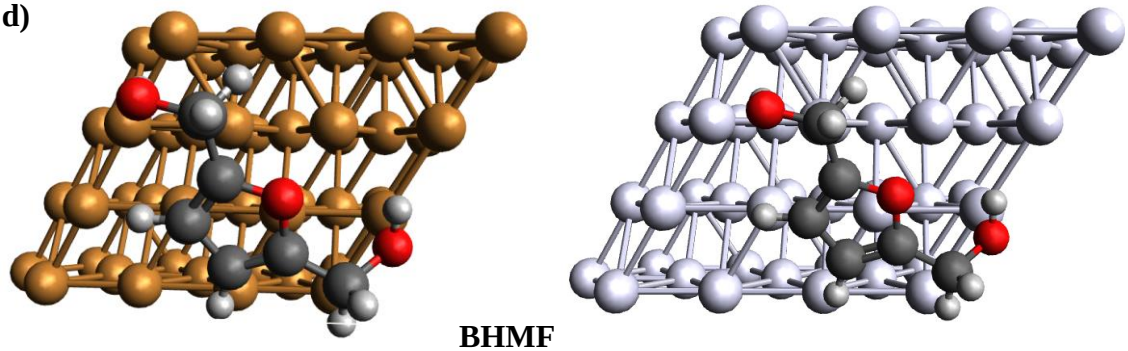

BHMF

e)

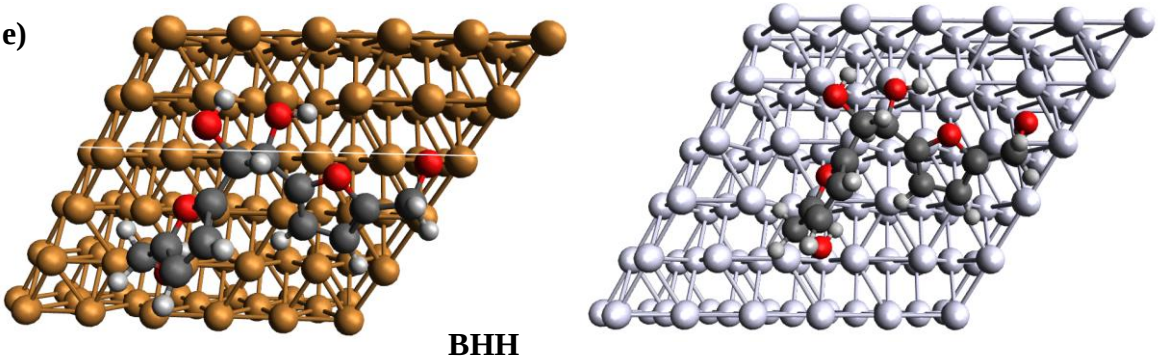

BHH

Figure 4.2. Top views of the most stable adsorption mode of HMF (**a**), I01 (**b**), I02 (**c**), BHMF (**d**), BHH (**e**) over Cu(111) (left panels) and Ag(111) (right panels). A 4X4, 3 layers supercell of each metal was considered, except for (**e**) where a 6x6 3 layers supercell was used.

In conclusion, a general trend is observed for the organic molecules adsorbed on Cu(111) or Ag(111). All the species are closer to the surface, with nearly flat adsorption, and are more distorted in the case of Cu(111). The most elongated bond is the carbonyl one, while the C-OH is usual poorly elongated in both cases. Ag(111) adsorbed compounds are also less stabilized than the Cu(111) counterparts with a difference around 0.1/0.2 eV (**Table 1**).

Table 1. Adsorption energies calculated using **Equation 3.1** on Cu(111) and Ag(111), p(4x4) symmetric 5L supercell, PBE functional and dDsC dispersion correction.

	E_{ads}/eV	
	Cu(111)	**Ag(111)**
HMF	-0.83	-0.76
BHMF	-1.06	-0.91
MF	-0.77	-0.69
MFA	-0.93	-0.83
BHH	-1.18	-1.23

4.3 Comparison between theoretical approaches

Both CHE and GC-DFT methodologies have been exploited in this work. In the following subsections the performances of both the theoretical approaches are compared, using the results for the hydrogen coverage and the energies of crucial reactions for both Cu(111) and Ag(111) surfaces, in order to find in which cases GC-DFT is worth using.

4.3.1 Hydrogen coverage

Since the ECH is held in an aqueous environment, HER can compete with it. Hydronium (or water) can react at the electrode (M), forming adsorbed hydrogen (H*) in a Volmer step. In HER, it can be followed by Tafel and Heyrovsky reactions, that lead to H_2 formation. Furthermore, if HAT is the preponderant mechanism, the Volmer step is shared between the two processes (i.e. HER and ECH). For these reasons, hydrogen coverage over Cu(111) and Ag(111) as a function of the electrode potential has been addressed in this work.

The hydrogen coverage has been investigated on a p(4x4), 5 layers, symmetric supercell. Both CHE and GC-DFT tests showed that the hydrogen atoms prefer to be adsorbed on threefold hollow sites, without any energetic differences between the *hcp* and *fcc* sites. Adsorbing 16 H in a p(4x4) cell, allows to reach a full monolayer (1 ML). The differential adsorption energies with the case of 8 H_2 free molecules have been computed for each case from a coverage of 1 ML to a coverage of 1/16 ML, at a pH = 9.2, for both the metallic surfaces. The influence of the electrode potential has been addressed using both CHE and GC-DFT approaches. Although the kinetics of the hydrogen adsorption is neglected, it is possible to assume that it varies as a function of the electrode potential with the same trend of the thermodynamics [46].

In the case of Cu(111), CHE results showed that the full coverage is the most favored one in the potential region between -1.50 V vs SCE to -0.90 V vs SCE. The hydrogen coverage goes down to 9/16 ML at -0.80 V vs SCE, and then a rapid decrease is observed, until the pristine surface at -0.70 V vs SCE is reached (**Figure 4.3.a**). GC-DFT results do not modify the conclusion reached with the CHE approach (**Figure 4.3.b**). Experimental LSVs performed on Cu/Cu foam in borate buffer (pH = 9.2) showed an onset for the HER at -1.15 V vs SCE that is a bit far from the computed value of -0.80 V vs SCE.

In the case of Ag(111), CHE results showed that the full coverage is the most favored one in the potential region between -1.50 V vs SCE and -1.30 V vs SCE. At -1.20 V vs SCE the coverage decreases to 9/16 ML, and continues the decrease until it reaches 0/16 at -1.10 V vs SCE (**Figure 4.3.b**). Here again, the trend is almost replicated by GC-DFT (**Figure 4.3.b**). The potential of -1.10 V vs SCE, at which the coverage starts increasing from 0/16, agrees well

with the experimental offset for HER of -1.15 V vs SCE observed with the LSV performed on Ag/Ag catalyst in borate buffer (pH = 9.2). These computational results suggest that Cu is more active toward the HER than Ag, such as also the experimental evidences indicate.

For the hydrogen coverage, CHE is enough to reach reliable results. The discrepancy with the experimental values for Cu(111) of the offset potential do not lie in this aspect of the modelling.

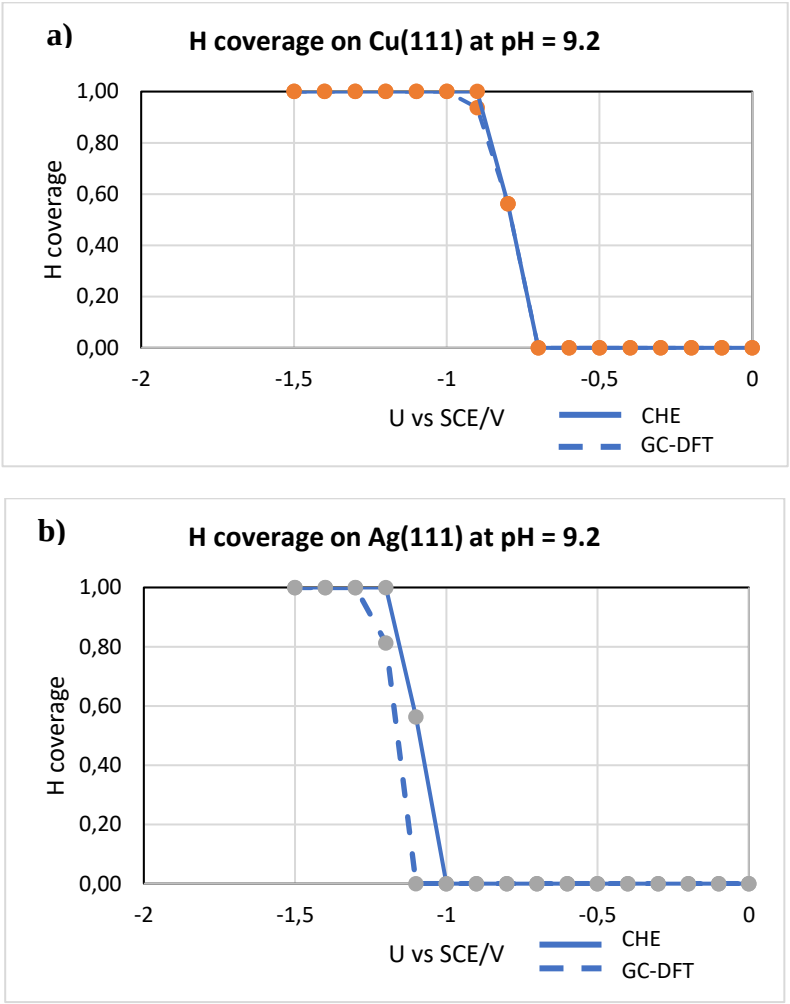

Figure 4.3. The thermodynamically favored hydrogen coverage for **(a)** Cu(111) and **(b)** Ag(111) p(4x4), 5 L, symmetric supercell as a function of the electrode potential at pH = 9.2. Continuous line refers to the trend calculated with the CHE approach, while the dotted one shows the evidences collected with the GC-DFT approach.

4.3.2 Hydrogen adsorbed reactions

Once the hydrogen atoms are adsorbed on the surface, they can interact each other (in HER) or with other intermediates (in HAT) formed over the electrocatalyst during the HMF-ECH. In this section the reaction of H* with the adsorbed oxygen (O*) and the adsorbed hydroxyl (OH*) are considered. These reactions are also involved inside the HMF-ECH reaction network

(**Figure 4.4**), and can be thermodynamically crucial steps. The free energy of these processes has been computed using CHE and GC-DFT for both Cu(111) and Ag(111) p(4x4) 5 layers symmetric supercells at the experimental conditions of -1.30 V vs SCE and pH = 9.2 (**Table 2**). As already shown in the previous section, for Cu(111) CHE and GC-DFT perfectly agree on the energy of H* formation. A value of -0.57 eV is obtained in both cases. Moving to OH* formation, CHE predicts a more exothermic reaction than GC-DFT. A difference of 0.43 eV is observed between the two computed values. For H2O* formation and desorption, CHE predicts instead less exothermic processes than GC-DFT.

For Ag(111), CHE and GC-DFT show a similar trend compared to the one discussed for Cu(111).

Table 2 The free energies (and their differences) computed at the CHE and GC-DFT level for the reactions indicated. Data are collected for Cu(111) p(4x4) 5 L symmetric supercell, at a potential of -1.30 V vs SCE and pH =9.2. The free energy is computed as explained in se 3.2. In the first columns "*" indicates species adsorbed over the metal surface. The values in red are the ones for which a difference of more than 0.1 eV is observed between CHE and GC-DFT.

	ΔG_r/eV		
Reaction	**CHE**	**GC-DFT**	**Δ(CHE–GC-DFT)**
$(H^+ + e^-)_{aq}$ + Cu → H*	-0.57	-0.57	0
H* + O* → OH* + Cu	-0.58	-0.15	-0.43
H* + OH* → H_2O* + Cu	0.08	-0.08	0.16
H_2O* → Cu + H_2O	-0.28	-0.42	0.14

The comparison between CHE and GC-DFT results for these simple reactions shows that, for both the metals, some appreciable differences can appear between the theoretical methods, especially for reactions where, intuitively, a relevant change in the surface dipole appears.

4.3.3 BHMF formation

Once CHE and GC-DFT performances for simple reactions have been analyzed, their results for the HMF-ECH must be compared to find the best methodology for the computation of the complete free energy profile. As an example, the results for the free energies of the reactive steps for BHMF formation are considered in this section. The reaction network (**Figure 4.4**) is a reduced version of the one shown in **Figure 4.1**.

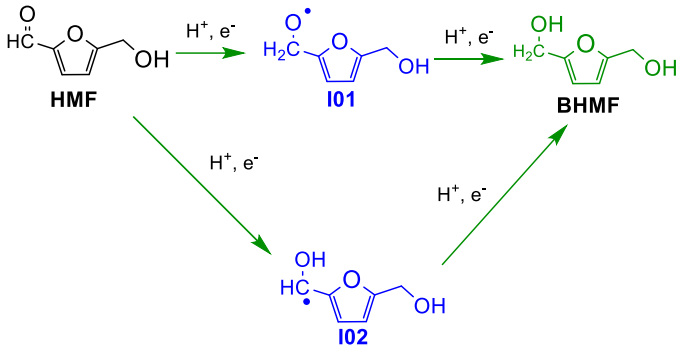

Figure 4.4. Reactive steps for the conversion of HMF into BHMF.

The free energies are all computed at the condition of -1.30 V vs SCE and pH = 9.2, for the metal p(4x4) 5 layers symmetrized supercell.

In the case of Cu(111), CHE and GC-DFT showed discrepancy on the adsorption energy of HMF and the desorption energy of BHMF. Looking at **Table 3**, for reaction 1 (R1) a difference of -0.51 eV is observed between the values predicted with the two methods, while for R6 a difference of 0.39 eV appears. CHE predicts an almost athermic adsorption of HMF and endothermic desorption of BHMF, instead GC-DFT predicts an endothermic adsorption of HMF and a slight exothermic desorption of BHMF. For all other reactions, except for R4, a difference of less than 0.1 eV is observed for the two approaches. A similar trend has been observed for Ag(111).

Table 3 The free energies (and their differences) computed at the CHE and GC-DFT level for the reactions indicated. Data are collected for Cu(111) p(4x4) 5L symmetric supercell, at a potential of -1.30 V vs SCE and pH =9.2. In the first columns "*" indicates species adsorbed over the metal surface. The values in red are the ones for which a difference of more than 0.1 eV is observed between CHE and GC-DFT.

		ΔG_r/eV		
	Reaction	**CHE**	**GC-DFT**	**Δ(CHE –GC-DFT)**
R1	HMF + Cu → HMF*	-0.05	0.46	-0.51
R2	HMF* + $(H^+ + e^-)_{aq}$ → I01*	-1.15	-1.08	-0.07
R3	HMF* + $(H^+ + e^-)_{aq}$ → I02*	-0.49	-0.54	0.05
R4	I01* + $(H^+ + e^-)_{aq}$ → BHMF*	-0.56	-0.74	0.18
R5	I02* + $(H^+ + e^-)_{aq}$ → BHMF*	-1.22	-1.28	0.06
R6	BHMF* → BHMF + Cu	0.28	-0.11	0.39

The trend of the energy for R1 and R6 as a function of the potential have been plotted and are shown in **Figure 4.5.** Since these ones are "chemical step", the CHE predicted energy is constant. In contrast, the GC-DFT ones change. In particular, HMF adsorption becomes more endothermic while using more cathodic potential, while BHMF desorption becomes more exergonic. Therefore, appreciable differences are observed between CHE and GC-DFT.

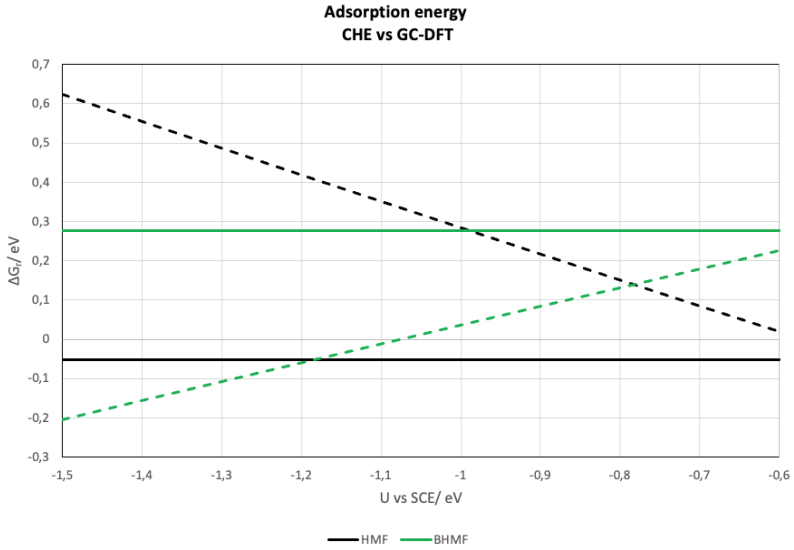

Figure 4.5. The adsorption energy of HMF (in black) and the desorption energy of BHMF (in green) over Cu(111) p(4x4) 5 L symmetric slab as a function of the potential for CHE and GC-DFT approach. The continuous line refers to CHE, while the dotted line refers to GC-DFT computed values.

Looking at **Table 3**, except for R4, the reaction for which the major discrepancies are observed are R1 and R6, both chemical steps and, in particular, adsorption/desorption processes. Also, for H_2O adsorption a discrepancy is observed, while no one for H adsorption (**Table 2**). For all these cases, an appreciable potential dependence appears and differences between CHE and GC-DFT are observed. Liu and co-workers have proposed that the potential dependence of an elementary reaction is related to the difference in the work function of the involved species at zero charge [47]. Michel and co-workers observed that in the case of HCOOH/CO_2 electrocatalytic reaction, the largest jump in the work function occurs for adsorption/desorption phenomena, which are also the steps more sensitive to the potential, for which they observed the major discrepancy between CHE and GC-DFT [6]. They also proved that the work function changes are correlated to the dipole moment of the adsorbates [6].

In **Table 4** the dipole of the adsorbate, the work function differences (between the bare slab and the slab with adsorbate), ΔW, and the discrepancy between CHE and GC-DFT predicted adsorption energy are showed. The greatest the dipole, the greatest the work function and also the discrepancy. These results agree with the trend observed in literature for other systems [5] [6].

Table 4 The dipole moment (μ) of the adsorbate along the z direction, in the case of a Cu p(4x4) 3L supercell, the work function difference ΔW (vs SHE) between the bare surface and the adsorbed surface and the value of the difference between the adsorption energy computed at the CHE level and the one computed at the GC-DFT level (Δ(CHE − GC-DFT)), at -1.30 V vs SCE, a pH of 9.2 for a Cu p(4x4) 5L symmetrized supercell for the chemical species in the first column.

	μ (z)/D	ΔW (vs SHE)/V	Δ(CHE – GC-DFT) eV
H*	-0.04	0.04	0.00
H2O*	-0.22	0.46	0.14
BHMF*	-0.38	0.61	0.39
HMF*	-0.55	0.87	0.51

As shown in section 2.3, within the GC-DFT framework the energy of a certain chemical species as a function of the potential is a parabola. Therefore, the reaction energy is a difference between parabolas, that can have vertexes more or less shifted one another, and different breadths. The vertex of the parabola is the work function (i.e. the potential of zero charge). In adsorption/desorption processes the two parabolas involved are the one of the bare surface and the one of the surface plus the adsorbate. The position of the last is driven by the dipole. In particular, the higher the dipole, the more work functions (i.e. the vertexes) differ, and a greater potential dependence is observed for a certain reaction. This observation agree with the data shown in **Table 4** and literature.

It can be concluded that GC-DFT is a useful tool for HMF-ECH computational study, in order to reach a detailed and more realistic description of the electrochemistry on metal electrodes. For this reason, in section 4.5 only GC-DFT energy profiles are shown.

4.4 Energy profiles of HMF-ECH

The reaction network investigated (**Figure 4.6**) is a restricted version of the one shown in **Figure 4.1**. The conversion of HMF into BHMF, two side reactions involving the C-O bond breaking (i.e. MF and MFA formation), and one involving the C-C bond formation (i.e. BHH formation) are included. The first three side reactions have been investigated on a p(4x4) supercell, while the latter, because of the dimension of the dimer, required a p(6x6) supercell.

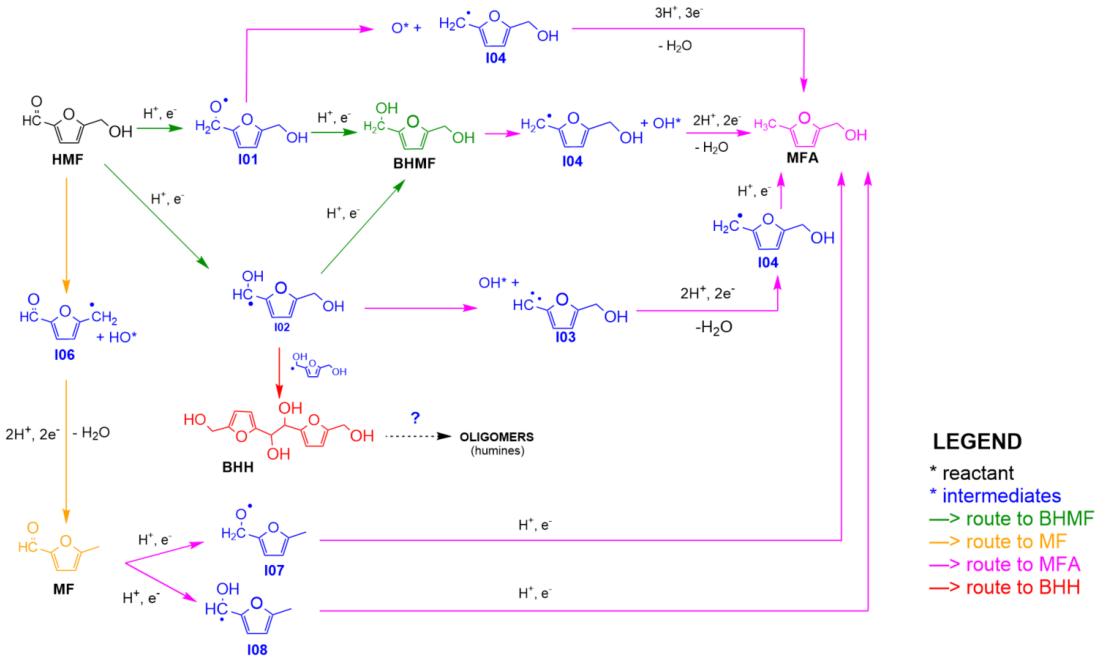

Figure 4.6. The investigated reaction network with green routes (i.e. BHMF formation), yellow routes (i.e. MF formation) and pink routes (i.e. MFA formation) studied on metallic p(4x4) 5L symmetric supercell. The red route (i.e. BHH formation) has been studied on metallic p(6x6) 5L symmetric supercell.

The following profiles are all computed at the GC-DFT level of theory.

4.4.1 Cu(111)

First the *route to BHMF* in **Figure 4.9** has been addressed. HMF can undergo a PCET either on the carbon or the oxygen of the carbonyl forming an alkoxy radical (**I01***) or an hydroxyalkyl radical (**I02***). Both the intermediates can be involved in a subsequent PCET forming BHMF For HMF/BHMF a theoretical Nernst potential of 0.03 V vs SCE has been computed. This value is quite near to the experimental one, that is -0.12 V vs SCE [48] [49]. At the experimental pH (i.e. 9.2), the equilibrium potential for HMF/BHMF becomes -0.58 V vs SCE The energy profile for the *route to BHMF* of the reaction network in **Figure 4.6** on

Cu(111) in this condition is shown in **Figure 4.7**. **I01*** formation is exergonic while **I02*** formation is strongly endergonic. An energy difference of 0.75 eV between the intermediate **I01*** and **I02*** is observed. In particular, the most stabilized intermediate is **I01*** that is formed after the transfer of one (H^+ + e^-) couple on the carbon of the carbonyl group. This alkoxy intermediate interacts with the metal surface using the oxygen of the C-O bond (see section 4.3). This feature is in line with the pronounced oxyphilic property of copper. The formation of **I02*** in this condition is thermodynamically disfavored, in contrast with **I01***. Instead BHMF* formation is thermodynamically favored from **I02*** but not from **I01***.

Using more cathodic potentials all the intermediates (except for HMF*) are stabilized, although **I01*** remains always the favored one. BHMF* formation becomes exergonic only at -0.66 V vs SCE, that is the thermodynamic overpotential at pH = 9.2 (**Figure 4.7**). The formation of **I01*** is exothermic, and BHMF formation from this intermediate is athermic. The formation of **I02***, instead, is endothermic, and an energy difference of 0.63 eV is observed between **I01*** and **I02***, less than the one at Nernst potential.

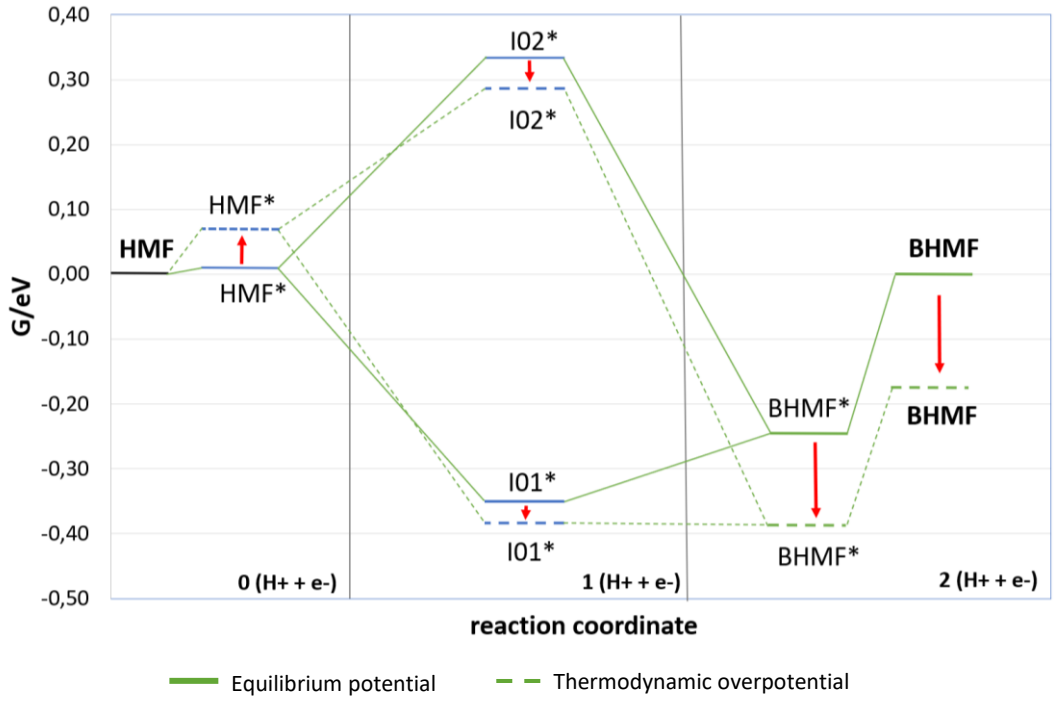

Figure 4.7. The reaction energy profile of HMF electrocatalytic hydrogenation to BHMF (*route to BHMF* in Figure 4.6) over Cu(111), evaluated with the GC-DFT approach, at the computed equilibrium potential (-0.58 V vs SCE; dotted lines) and at the thermodynamic overpotential at pH = 9.2 (-0.66 V vs SCE; continuous line) for a p(4X4) 5L symmetrized cell. The * indicates an adsorbed compound. Only the free energies of the chemical species are shown (no transition states). They are organized as a function of the number of H^+ + e^- couples transferred before their formations. The red arrows indicate the effect of the application of an overpotential.

Once the thermodynamical overpotential has been defined, the free energy profile at the experimental condition of -1.30 V vs SCE and pH = 9.2 has been plotted (**Figure 4.8**). The reaction network has been enlarged to include BHH formation, meaning that both the *route to BHMF* and *route to BHH* in **Figure 4.8** have been included.

Moving to more cathodic potentials, the intermediates are generally stabilized since the electrochemical potential of the ($H^+ + e^-$) couple becomes more positive, although the presence of the charged surface can either stabilize or destabilize the intermediates. Focusing on the green path, the adsorption energy of HMF becomes endergonic. The formation of both **I02*** and **I01*** is exergonic. Both the intermediates are more stabilized and the energy difference between them (0.64 eV) is almost the same as compared to the thermodynamic overpotential condition. The formation of BHMF* from both the intermediates is exothermic. An energy reaction of -1.05 eV is observed for the formation of BHMF* from **I01*** and of -1.28 eV from **I02***. These strongly exergonic reactions indicate that there are not thermodynamical reasons to use such reducing condition to make the reaction happen.

Focusing on the red path, the reaction energy for the formation of ½ BHH*, calculated on a p(6x6) supercell, is -0.58 eV, therefore the reaction is spontaneous, in agreement with the experimental evidence. The desorption of BHH is endergonic, and only slightly changes as a function of the electrode potential.

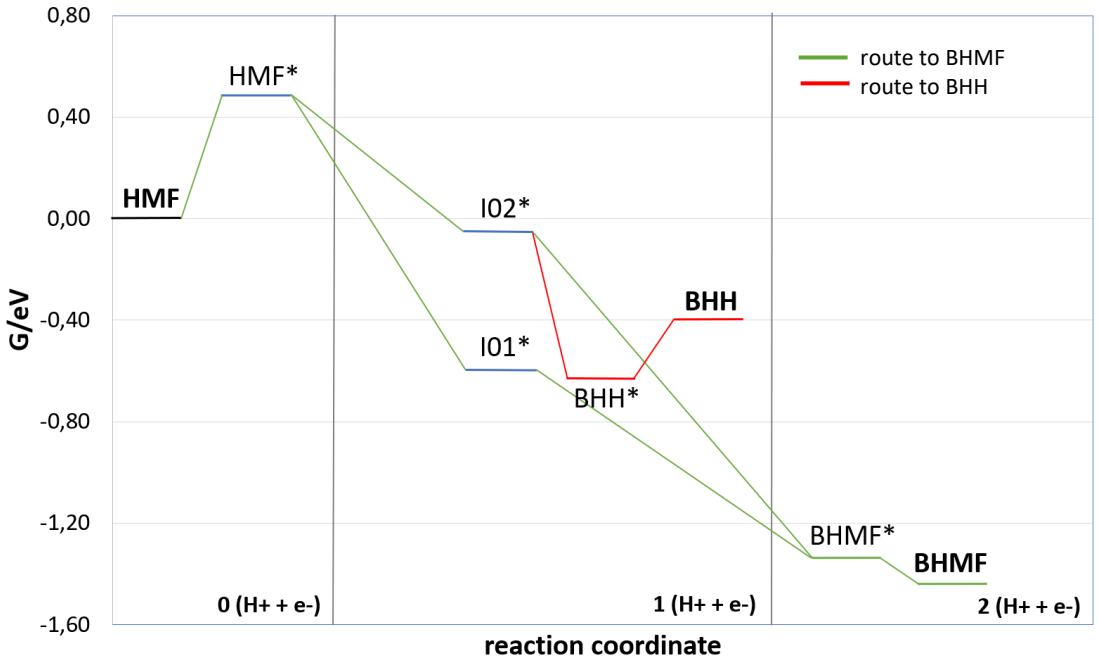

Figure 4.8. The reaction energy profile of HMF electrocatalytic hydrogenation over Cu(111), computed with GC-DFT approach, at the potential of -1.30 V vs SCE and a pH = 9.2, on a p(4x4) 5L symmetric supercell for the route to BHMF and on a p(6x6) 5L symmetric supercell for the route to BHH. The *route to BHMF* and *route to BHH* of **Figure 4.6** are considered. (for the manual see the caption of **Figure 4.7**).

Finally, the reaction network has been enlarged to include the *route to MF* and the *route to MFA* (see **Figure 4.6**). The free energy profiles at the experimental condition of -1.30 V vs SCE and pH = 9.2 have been plotted (**Figure 4.9**). Considering the *route to MF* all the reactions are strongly exergonic. MF can further be converted to MFA, through the formation of **I07***. **I01***, **I02*** and BHMF* instead cannot further be converted into MFA, since the first reactive steps along these routes (C-O breaking) are thermodynamically disfavored at this potential. Therefore, MFA is likely produced only from MF. Since MF and MFA are more stabilized than BHMF, this one is not the thermodynamical product.

The energy profiles for Cu(111) showed that the formation of all the products considered (BHMF, MFA, MF) is thermodynamically allowed at -1.30 V vs SCE and pH = 9.2, as also the experimental results revealed.

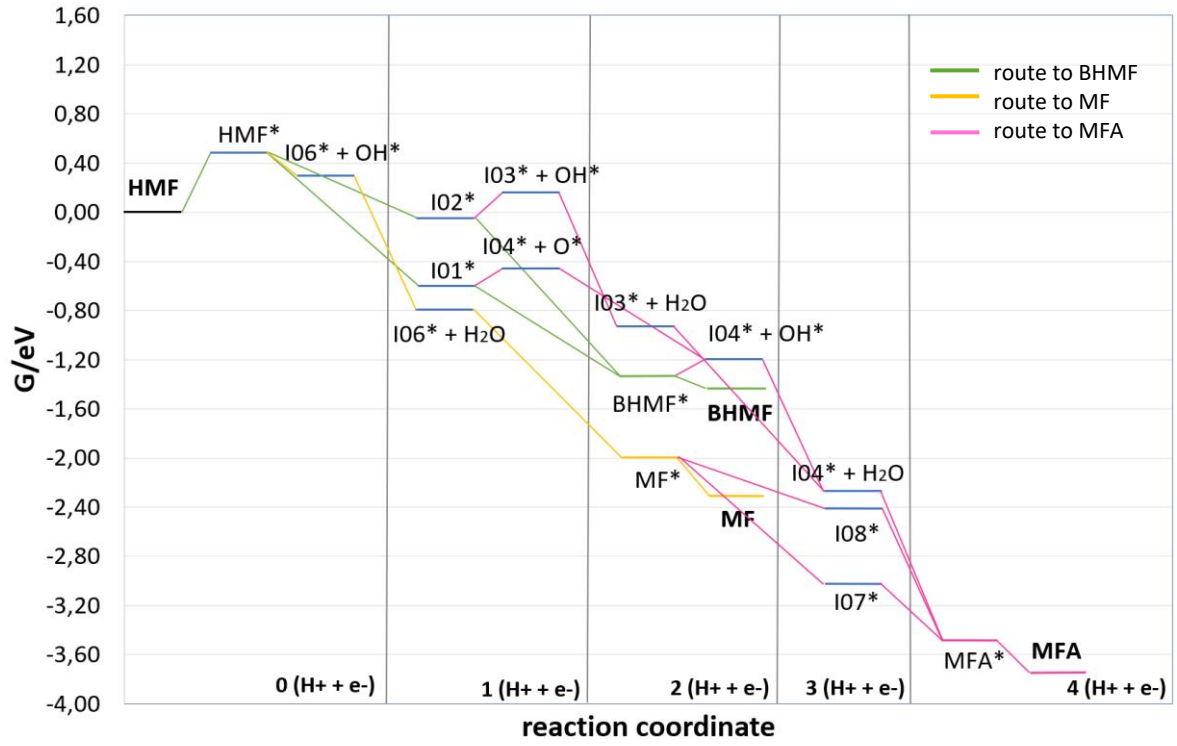

Figure 4.9. The reaction energy profile of HMF electrocatalytic hydrogenation over Cu(111), evaluated with GC-DFT approach, at the potential of -1.30 V vs SCE and a pH = 9.2, for a 4x4 5L symmetrized supercell. The *route to BHMF*, the *route to MF* and the *route to MFA* of Figure 4.6 are considered.

4.4.2 Ag(111)

The energy profile for the *route to BHMF* of the reaction network in **Figure 4.6** at the equilibrium potential at pH = 9.2 (-0.58 V vs SCE) on Ag(111) is shown in **Figure 4.10**. The formation of both the intermediates **I01*** and **I02*** is endergonic. **I01*** is the most stabilized one, as for the case of Cu(111). **I01*** and **I02*** are quite near in energy (0.03 eV difference). This result can be ascribed to the less oxyphilic characteristic of Ag compared to Cu. The reaction formation of BHMF* from both the intermediates is exergonic.

At -0.76 eV vs SCE at pH = 9.2, the formation of BHMF* becomes thermodynamically allowed. This condition corresponds to the thermodynamic overpotential, that is just 0.1 V more cathodic than the one predicted for Cu(111). The energy gap between **I01*** and **I02*** is 0.45 eV, greater than in the condition of the equilibrium potential.

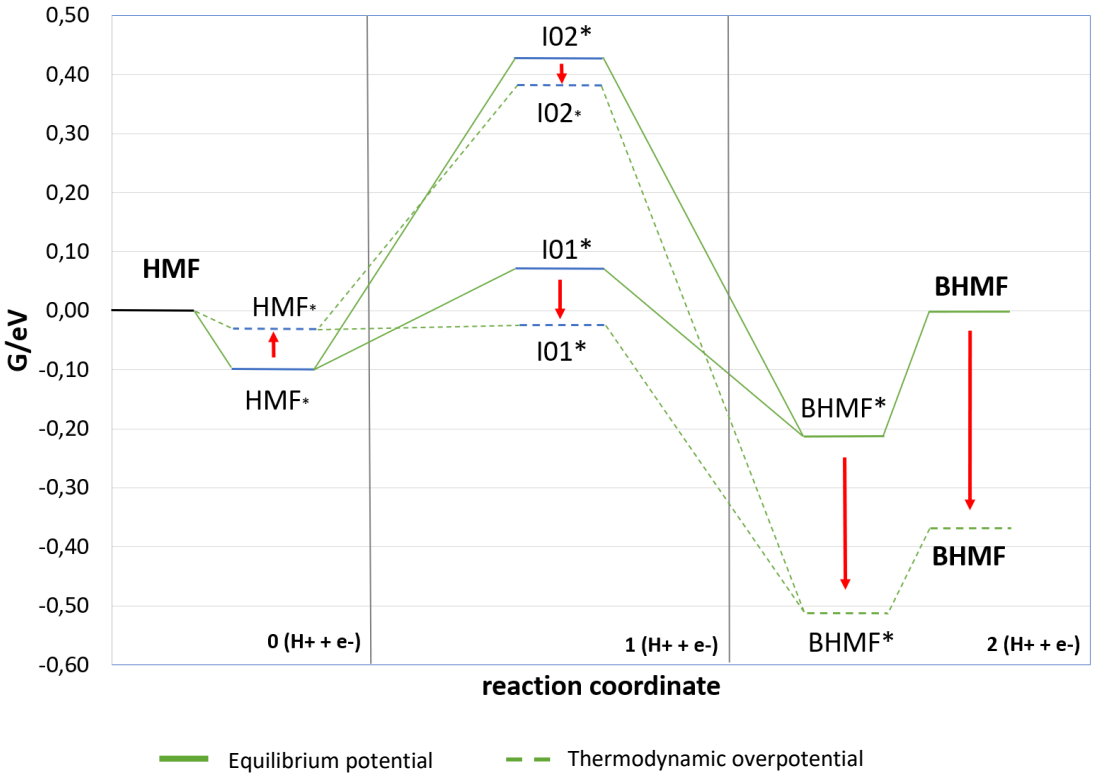

Figure 4.10. The reaction energy profile of HMF electrocatalytic hydrogenation to BHMF (*route to BHMF* in **Figure 4.6**) over Ag(111), evaluated with the GC-DFT approach, at the computed equilibrium potential (-0.58V vs SCE; dotted lines) and at the thermodynamic overpotential (-0.76 V vs SCE; continuous line) at pH = 9.2 for a p(4x4) 5L symmetric supercell. (for the manual see the caption of **Figure 4.7**)

Once the thermodynamical overpotential has been defined, the free energy profile at the experimental condition of -1.30 V vs SCE and pH = 9.2 has been plotted (**Figure 4.11**). The reaction network has been enlarged to include BHH formation, meaning that both the *route to BHMF* and *route to BHH* in **Figure 4.6** have been included.

Focusing on the green path, the adsorption process of HMF is athermic. The formation of both **I02*** and **I01*** is exergonic. Their energy difference is increased as compared to the one at thermodynamic overpotential (0.55 eV instead of 0.45 eV). The formation of BHMF* from both the intermediates is exergonic. An energy reaction of -0.73 eV is observed for the formation of BHMF* from **I01*** and of -1.28 eV from **I02***. This first reaction energy differs from the one computed for Cu(111) that is more exergonic, instead the second one is identical. According to the computed energy profile, at -1.30 V vs SCE the formation of BHMF for Ag(111), as for the case of Cu(111) is strongly exergonic, and therefore the use of such a reducing potential is not justified by thermodynamical considerations. BHMF desorption is endergonic.

Considering the red path, the reaction energy for the formation of ½ BHH* is -0.64 eV, therefore it is spontaneous. This energy is quite identical to the one computed for Cu(111) (-0.58 eV), as also the desorption energy of BHH*.

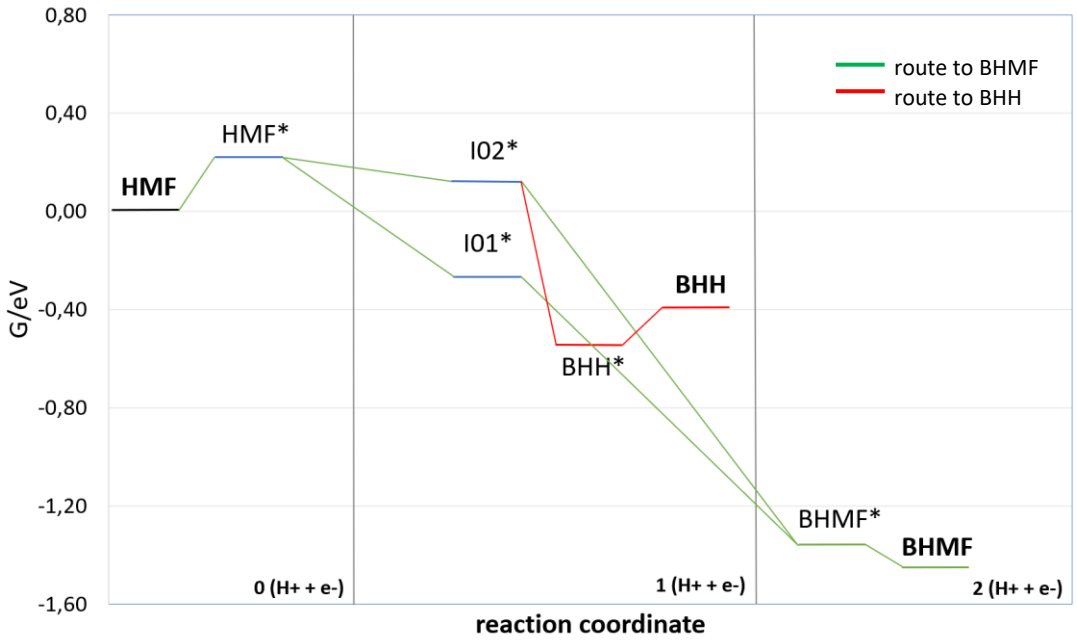

Figure 4.11. The reaction energy profile of HMF electrocatalytic hydrogenation over Ag(111), computed with GC-DFT approach, at the potential of -1.30 V vs SCE and a pH = 9.2, on a p(4x4) 5L symmetric supercell for the route to BHMF and on a p(6x6) 5L symmetric supercell for the route to BHH. The *route to BHMF* and *route to BHH* of **Figure 4.6** are considered.

As for the case of Cu(111), the reaction network has been enlarged to include the *route to MF* and the *route to MFA* (see **Figure 4.6**). The free energy profile at the experimental condition of -1.30 V vs SCE and pH = 9.2 has been plotted (**Figure 4.12**).

Focusing on the yellow route, the first step is slightly endergonic. All the other steps instead are strongly exergonic. The only route thermodynamically allowed for MFA formation is the one starting from MF, whose reactive steps are all exergonic; the routes from **I01***, **I02*** and BHMF* are thermodynamically disfavored, as for the case of Cu(111).

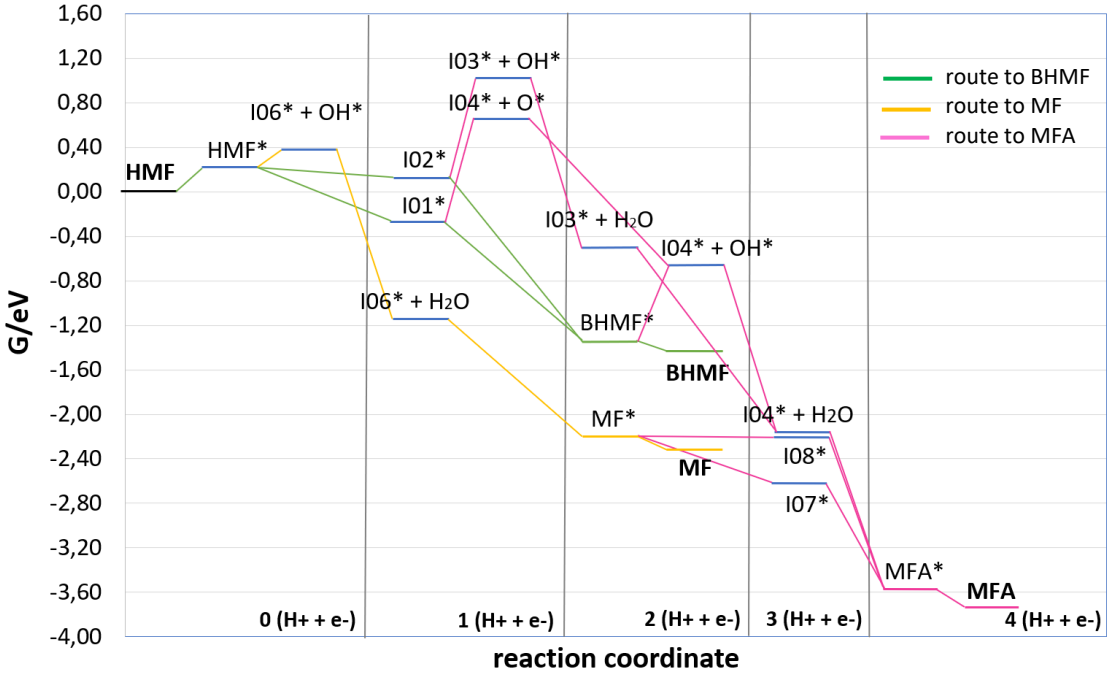

Figure 4.12. The reaction energy profile of HMF electrocatalytic hydrogenation over Ag(111), evaluated with GC-DFT approach, at the potential of -1.30 V vs SCE and a pH = 9.2, for a 4x4 5L symmetrized supercell. The *route to BHMF*, the *route to MF* and the *route to MFA* of **Figure 4.6** are considered.

4.4.3 Cu(111) vs Ag(111)

The energy profiles computed for Cu(111) and Ag(111) highlight some interesting differences between the two metals, which allow rationalizing the experimental evidences.

Cu(111) showed a thermodynamical overpotential of -0.66 V vs SCE, while for Ag(111) it is -0.76 V vs SCE. A difference of only 0.1 V is observed. This result agrees with the experimental evidences, which suggested the same activity for Cu and Ag electrocatalyst toward HMF-ECH. As observed in section 4.3, the adsorption energies for all the reaction intermediates are always a bit more exothermic (around 0.1/0.2 eV) on Cu(111) than on Ag(111). For both metals, alkoxy intermediates (**I01*** and **I07***) are more stabilized than hydroxyalkyl radical (**I02*** and **I08***). This feature is a consequence of the oxyphilic character of the metals. Since Ag is less

oxyphilic than Cu, the alkoxies intermediates are less stabilized on Ag. Considering the couples **I01*** and **I02*** and the couple **I08*** and **I07***, in both cases the ones who interact through the oxygen radical are more stabilized. The difference between the two intermediates of the couples is bigger for Cu(111) than for Ag(111), and it slightly changes as a function of the electrode potential. **I01*** and **I02*** are particularly crucial intermediates, since them both are involved in BHMF formation. Moreover, the latter is involved also in BHH formation, which here is supposed to be involved in humines formation. Experimentally BHH and humines are the main side products. Reducing the selectivity towards these side products implies improving the selectivity toward BHMF. Therefore, considering only thermodynamics, a high stabilization of **I01*** and a high destabilization of **I02*** are desired. In the case of Ag(111), at the experimental condition (-1.3 V vs SCE and pH = 9.2) the formation of **I02*** is almost athermic (0.1 eV), while the subsequent formation of BHH is strongly exergonic (**Figure 4.13)** . The formation of both **I01*** and BHMF* are also exergonic. In the case of Cu(111), the formation of both the intermediate **I01*** and **I02*** is exergonic (and also the subsequent reactions). The different stabilization of **I02*** con Cu(111) and Ag(111) could explain why more humines are formed for Cu electrocatalyst, and why Ag electrocatalyst showed better performance in BHMF selectivity. If **I02*** is less stabilized, as for the case of Ag, less BHH should be formed. Since the experimental evidences suggested that humines are formed from BHH, this means that less humines will be formed.

Moving to more anodic potential, **I01*** and **I02*** formation becomes less exothermic for both the metals (**Figure 4.14**). In the case of Ag, the formation of **I02*** becomes endothermic at potential that is possibly enough reducing that the reaction can be performed in a reasonable time.

In the case of Ag(111) at -1.30 V vs SCE the energy for formation of **I02*** is -0.10 eV, while moving to -1.10 V vs SCE it becomes 0.12 eV. The accuracy of the computational method on the potential values is not very high, but a trend is observed. A similar trend happens also in the case of Cu(111), although the reaction remains always exothermic.

For I01* formation the use of more anodic potential reduces the energy for the reaction, but it remains always exothermic for both Cu(111) and Ag(111).

Further experimental tests should explore these theoretical predictions, in order to validate our theoretical model.

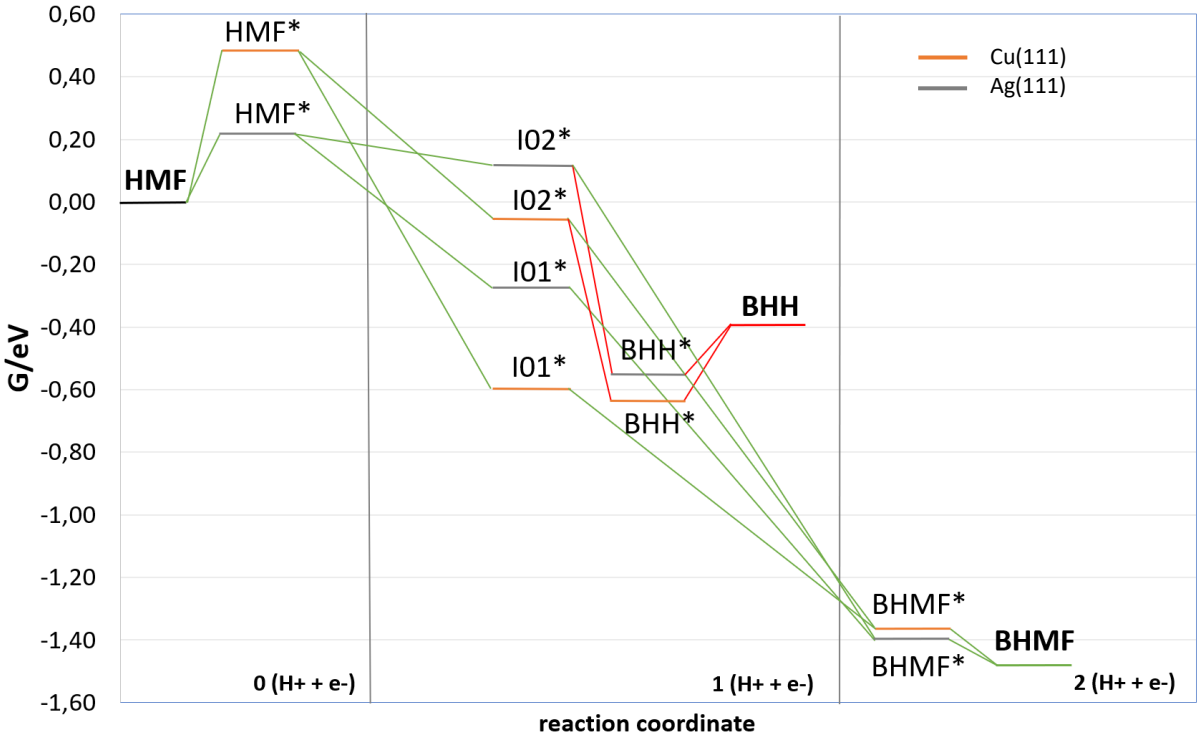

Figure 4.13. The energy profile for BHMF formation (BHMF route in **Figure 4.7**) for both Cu 111) and Ag(111), evaluated with GC-DFT approach, at the potential of -1.30 V vs SCE and a pH = 9.2, for a p(4x4) 5L symmetric supercell is shown. The orange bars refer to the intermediates formed over Cu(111), while the grey ones refer to Ag(111).

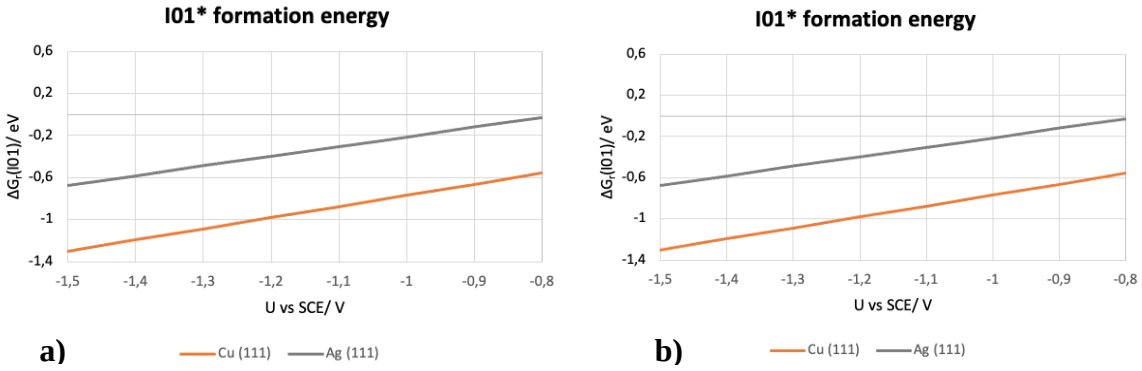

Figure 4.14. Energy formation of I01* **(a)** and I02* **(b)** computed with GC-DFT for a p(4x4) 5L symmetric supercell of Cu(111) and Ag(111). The orange lines refer to Cu(111), while the grey line refers to Ag(111).

The energy profiles for HMF-ECH over Cu(111) at the experimental conditions showed that the formation of all products (BHMF, BHH, MFA, MF) is thermodynamically allowed, in agreement with the experimental evidences. MFA can only be formed from MF, since all the reactive steps involving C-O bond breaking (except for HMF → I06* + OH*) are endergonic. In the case of Ag(111), the formation of BHMF and BHH is thermodynamically allowed; instead the first step of MF formation is slightly endergonic (0.16 eV), and all the other steps involving a C-O bond breaking are highly endergonic. Since MFA can be formed only from MF, both the products should not be formed. Experimental results, instead, showed formation of these compounds, although just in traces. This "discrepancy" can be explained considering that the blocking reaction is only slightly endergonic, and the computational error on such a small number can greatly impact the final interpretation.

5 Conclusions

Four main goals have been addressed in this work: 1) comparison between the performances of CHE and GC-DFT approaches in the study of the HMF-ECH process; 2) obtain insights into the reaction mechanism of HMF electrocatalytic hydrogenation over Cu(111) and Ag(111) surfaces; 3) rationalization of the experimental evidences; and 4) definition of criteria for the design of better catalysts.

A hypothetical reaction network has been defined for HMF-ECH, including the products that have been experimentally revealed. Among the two hypothetical mechanisms (PCET and HAT) proposed in literature, only PCET has been considered inside the reaction network built in this work. This choice is a weakness of our investigation, which will need to be completed in future studies. In fact, although the mechanism involved in HMF-ECH has not been yet clarified in literature, it has been experimentally shown that in the case of furfural both the PCET and HAT are involved.

By performing periodic DFT calculations and using the CHE and GC-DFT theoretical approaches, the energy profiles for the hypothetical reaction network as a function of the electrode potential have been computed. The performances of the two theoretical approaches have been compared, showing major discrepancy between the predicted energies for adsorption/desorption reactions. We have observed that, as the dipole of the metallic surface increases, also the discrepancy increases, as it was also observed before in literature [5] [6]. This trend can be explained considering that at the CHE level of theory the adsorption/desorption energy is constant by definition, while at the GC-DFT level of theory it is defined as a difference between two parabolas associated to the energy of the adsorbate and the energy of the slabs as a function of the electrode potential. The reciprocal shift of the parabolas is controlled by the dipole of the adsorbate (in particular the dipole influences the work function, i.e. the vertex of the parabola). The more the parabolas are shifted, the more the adsorption/desorption energy shows a potential dependence and, as a consequence, an appreciable difference with respect to the value predicted by CHE (that is not potential dependent). In this work we showed that, in the case of HMF-ECH, GC-DFT proved itself as a necessary tool to refine CHE profiles.

The energy profiles have been built plotting the free energy of each intermediate as a function of the number of ($H^+ + e^-$) transferred, at specific electrode potentials. The kinetics of the reaction network has not been addressed in this work. Therefore, all the conclusions are based just on thermodynamical considerations.

The energy profiles computed at the experimental conditions (U = -1.3 V vs SCE and pH = 9.2) showed that for both Cu(111) and Ag(111), the formation of BHMF, BHH, MFA and MF is thermodynamically allowed. This evidence agrees with the experimental finding of all these products for both Cu/Cu and Ag/Ag foam electrocatalysts. The energy profiles showed that BHMF is not the thermodynamical product, since MF and MFA are more stable than BHMF. Furthermore, the profiles suggested that MFA is only formed from MF, for both metallic surfaces, as it was also suggested in literature for the case of copper [45]. The possible conversion routes of **I01***, **I02*** and BHMF into MFA are thermodynamically disfavored, since in all the three cases the steps which involve C-O bond breakings are endergonic, for both Cu(111) and Ag(111). In conclusion, within the approximation of our model (i.e. only PCET mechanism and only thermodynamis), important insights into the reaction mechanism of HMF-ECH over Cu(111) and Ag(111) have been obtained, reaching the first target of this work.

In order to rationalize the experimental evidences collected at the University of Bologna, the activity of Ag and Cu towards HER has been addressed as a first step. This reaction is quite crucial since it can compete with HMF-ECH, reducing the faradaic efficiency. Furthermore, if HAT mechanism is involved, the Volmer step is shared between HMF-ECH and HER, meaning a competition for the reactant (i.e. H*) and not only for the electron transfer. The computational study of the coverage over Cu(111) and Ag(111) revealed that Cu has a higher activity toward HER, since the coverage of H* decreases starting from a more anodic potential as compared to Ag, in agreement with the experimental evidence. The LSVs perfomed in the borate buffer for Cu and Ag electrocatalysts showed a more anodic potential and a greater current density decrease for Cu than Ag, meaning a higher activity towards HER for copper.

Subsequently the activity of the metals towards HMF-ECH has been addressed. A thermodynamic overpotential for HMF/BHMF of -0.66 V vs SCE has been computed for Cu(111) and of -0.76 V vs SCE for Ag(111). The two values are quite near and suggest almost the same activity of the two metals towards HMF-ECH. Also, this evidence finds a match with experimental results. LSVs performed in a solution of HMF 0.1 M in borate buffer, show almost the same offset potential and the same current density decrease for Cu and Ag electrocatalysts. The computed energy profiles showed that, moving to more cathodic potential, the formation of BHMF for both Cu(111) and Ag(111) becomes exergonic, and at a potential -1.3 V vs SCE (i.e. the electrode potential experimentally used) the reaction is strongly exergonic. This evidence suggests that our set of computations is not enough to explain why such a reducing potential is experimentally required to reach good performances in the selective conversion of HMF into BHMF. Possibly, future simulations of kinetics overpotential, kinetics

of the hydrogen transfer, and HAT mechanism will provide a more complete and clear picture. Moreover, the overpotential can be also due to other reasons that lies not on the atomic scale (e.g. concentration and/or resistance overpotential).

Another important experimental evidence is the different performance of Cu(111) and Ag(111) in humines formation. Although the oligomerization has not been explicitly included in the explored reaction network, assuming that humines formation is subsequent to BHH formation, our network could still shed a light on it. Since BHH is formed from **I02***, this intermediate is crucial in driving the formation of BHH, and humines subsequently. **I02*** is involved in both BHMF and BHH formation, while its C-O bond breaking that leads to MFA has been shown to be thermodynamically not allowed on Cu(111) and Ag(111). For both metals this intermediate is always less stable than **I01***, the other intermediate that leads to BHMF. This is an interesting result, since our main target is to increase the selectivity to BHMF and decrease the one to BHH and humines. For this reason, the condition in which **I02*** is less stable and **I01*** is more stable are the desired ones. The computed free energy profiles showed that at the experimental conditions **I02*** is less stable on Ag than Cu, and its formation is almost athermic on Ag(111). Since **I02*** forms BHH, which we assume can further oligomerize, it can be expected that the humines formation is less favored in the case of Ag than Cu, in line with the experimental evidences. In conclusion, thermodynamics considerations allowed us to rationalize most of the experimental evidences.

Finally, the computed energy profiles also suggested some possible criteria to improve the performance of the catalysts. Moving to more anodic potential, **I02*** formation becomes less favored, meaning that from a thermodynamical point of view also BHH and humines formation should become disfavored. Although in this condition the reaction becomes slower, some tests should be performed to check how the selectivity towards the main products changes. Furthermore, if the stabilization of **I02*** and humines formation showed to be correlated, providing a possible (simple) criterium for the screening of new catalysts.

In conclusion, the main targets for this work have been achieved, despite some experimental findings have not been fully rationalized by the computational results. As a future outlook our model must be extended, including also the computation of the activation barriers, at least for the reactive steps involved in BHMF and BHH formation. Also, the HAT mechanism should be addressed, in order to reach a more complete overview of HMF-ECH.

6 Bibliografia

[1] G. S. de Luna, P. H. Ho, A. Lolli, F. Ospitali, S. Albonetti, G. Fornasari e P. Benito, «Ag electrodeposited on Cu open-cell foams for the selectrive electroreduction of 5-hydrpxymethylfurfural,» *ChemElectroChem,* vol. 7, pp. 1238-1247, 2020.

[2] G. S. deLuna, P. H. Ho, A. Sacco, S. Hernàndez, J.-J. Velasco-Vélez, F. Ospitali, A. Paglianti, S. Albonetti, G. Fornasari e P. Benito, «AgCu bimetallic electrocatalysts for the reduction of biomass-derived compounds,» *ACS Applied Materials and Interfaces,* vol. 13, pp. 23675-23688, 2021.

[3] G. S. deLuna, A. Sacco, S. Hernandez, F. Ospitali, S. Albonetti, G. Fornasari e P. Benito, «Insight into the electrochemical reduction of 5-hydroxymethylfurfural at high current densities,» *ChemSusChem,* pp. e202102504-9, 2022.

[4] R. Réocroux e C. Michel, «Rational design of heterogeneous catalysts for biomass conversion - Inputs from computational chemistry,» *Curren Opinion in Green and Sustainable Chemistry,* vol. 10, pp. 51-59, 2018.

[5] H. Liu, T.-H. Lee, Y. Chen, E. W. Cochran e W. Li, «Paired electrolysis of 5-(hydroxymethyl)furfural in flow cells with high performance oxide-derived silver cathode,» *Green Chemistry,* n. 14, 2021.

[6] S. N. Steinmann, C. Michel, R. Schwiedernoch, J.-S. Filhol e P. Sautet, «Modeling the HCOOH/CO2 electrocatalytic reaction: when deteils are key,» *ChemPhysChem,* vol. 16, n. 11, pp. 2307-2311, 2015.

[7] P. T. Anastas e J. C. Warner, Green Chemistry Theory and Practice, New York: Oxfor University Press, 1998.

[8] P. Tundo, P. Anastas, D. Black, J. Breen, T. J. Collins, S. Memoli, J. Miyamoto, M. Polyakoff e W. Tumas, «Synthetic patways and processes in green chemistry. Introductory overview,» *Pure and Applied Chemistry,* vol. 72, n. 7, pp. 1207-1228, 2000.

[9] S. A. Akhade, «Electrocatalytic Hydrogenation of Biomass-Derived Organics: A Review,» *Chemical Reviews,* vol. 120, pp. 11370-11419, 2020.

[10] L. Hu, J. Xu, S. Zhou, A. He, X. Tang, L. Lin, J. Xu e Y. Zhao, «Catalytic advances in the production and application of biomass-derived 2,5-dihydroxymethylfuran,» *ACS Catal.,* vol. 8, pp. 2959-2980, 2018.

[11] A. S. May e E. J. Biddinger, «Strategies to control electrochemical hydrogenation and hydrogenolysis of furfural and minimize undesired side reactions,» *ACS Catal.,* vol. 10, pp. 3212-3221, 2020.

[12] A. Plucksacholatarn, B. Tharat, S. Suthirakun, K. Faungnawakij e A. Junkaew, «Theoretical insight into the interaction on Ni and Cu surfaces for HMF hydrogenation: a density functional theory study,» *New J. Chem,* vol. 45, pp. 21543-21552, 2021.

[13] R. Gunawan, H. S. Cahyadi, R. Insyani, S. K. Kwak e J. Kim, «Density functional theory investigation of the conversion of 5-hydorxymethylfurfural into 2,5-dimethylfuran over Pd(111) , Cu(111), and Cu3Pd(111) surfaces,» *J. Phys. Chem. C,* vol. 125, n. 19, pp. 10295-10317, 2021.

[14] K. I. Galkin e V. P. Ananikov, «When will 5-hydroxymethylfurfural, the "Sleeping giand" of sustainable chemistry, awaken?,» *ChemSusChem,* 2019.

[15] X. Shang, Y. Yang e Y. Sun, «Electrohydrodimerization of biomass-derived furfural generates a jet fuel preucursor,» *Green Chemistry,* vol. 22, pp. 5395-5401, 2020.

[16] D. K. Lee, S. R. Kubot, A. N. Janes, M. T. Bender, J. Woo, J. R. Schmidt e K.-S. Choi, «The impact of 5-hydroxymethylfurfural (HMF)-metal interactions on the electrochemical reduction pathways of HMF on various metal electrodes,» *ChemSusChem,* vol. 14, pp. 4563-4572, 2021.

[17] J. J. Roylance, T. w. Kim e K.-S. Choi, «Efficient and selective electrochemical and photoelectrochemical reduction of 5-hydroxymethylfurfural to 2,5-bishydroxymethylfuran using water as the hydrogen source,» *ACS Catalysis,* vol. 6, pp. 1840-1847, 2016.

[18] X. H. Chadderdon, D. J. Chadderdon, T. Pfennig, B. H. Shanks e W. Li, «Paired electrocatalytic hydrogenation and oxidation of 5-hydroxymethylfurfural for efficient production of biomass-derived monomers,» *Green Chem.,* vol. 21, pp. 6210-6219, 2019.

[19] P. Nilges e U. Schroder, «Electrochemistry for biofuel generation: production of furans by electrocatalatytic hydrogenation of furfurals,» *Energy & Enviromental Science,* n. 10, 2012.

[20] N. Ramaswamy e S. Mukerjee, «Understanding of Electrocatalysis of Oxygen Reduction,» *Advances in Physical Chemistry,* vol. 2012, pp. 1-17, 2012.

[21] K. Chan e J. K. Nørskov, «Electrochemical Barriers Made Simple,» *J. Phys. Chem. Lett.,* vol. 6, n. 14, pp. 2663-2668, 2015.

[22] A. H. Bard e L. R. Faulkner, Electrochemical methods: fundamentals and applications, Wiley, 1980.

[23] K. S. Exner e H. Over, «Kinetics of electrocatalytic reactions from fist-principles: a critical comparison with the ab initio thermodynamics approach,» *Account of chemical research*, vol. 50, pp. 1240-1247, 2017.

[24] R. Sundararaman e T. A. Arias, «Joint and grand-canonical density-functional theory,» in *Atomic-Scale Modelling of Electrochemical Systems*, Wiley, 2022, pp. 139-169.

[25] J. Nørskov, J. Rossmeisl, A. Logadottir, L. Lindqvsit, J. R. Kitchin, T. Bligaard e H. Jònsson, «Origin of the Overpotential for Oxygen Reduction at a Fuel-Cell Cathode,» *J. Phys. Chem. B*, vol. 108, pp. 17886-17892, 2004.

[26] N. Abidi, K. R. G. Lim, Z. W. Seh e S. N. Steinmann, «Atomistic modeling of electrocatalysis: Are we there yet?,» *WIREs Computational Molecular Science*, vol. 11, n. 3, p. e1499, 2021.

[27] R. Sundararaman, W. A. Goddard e T. A. Arias, «Grand canonical electronic density-functional theory: Algorithms and applications to electrochemistry,» *The Journal of Chemical Physics*, vol. 146, pp. 114104-13, 2017.

[28] M. M. Melander, T. T. Laurila e K. Laasonen, Atomic-scale modelling of electrochemical systems, Wiley, 2022, pp. 139-169.

[29] S. A. Petrosyan, A. A. Rigos e T. A. Arias, «Joint Density-Functional Theory: Ab initio Study of Cr2O3 Surface Chemistry in Solution,» *J. Phys. Chem. B*, vol. 109, n. 32, pp. 15436-15444, 2005.

[30] K. Mathew, R. Sundararaman e K. Letchworth-Weaver, «Implicit solvation model for density-functional study of nanocrystal surfaces and reaction pathways,» *The Journal of Chemical Physics*, vol. 140, pp. 084106-8, 2014.

[31] K. Mathew, V. S. C. Kolluru, S. Mula, S. N. Steinmann e R. G. Hennig, «Implicit self-consisten electrolyte model in plane-wave density-functional theory,» *The Journal of Chemical Physics*, vol. 151, pp. 234101-8, 2019.

[32] N. Abidi e S. N. Steinmann, «How are transition states modeled in heterogeneous electrocatalysis?,» *Current Opinion in Electrochemistry*, vol. 33, p. 100940, 2022.

[33] «VASP,» [Online]. Available: https://cmp.univie.ac.at/research/vasp/. [Consultato il giorno April 2023].

[34] «The VASP Manual,» [Online]. Available: https://www.vasp.at/wiki/index.php/The_VASP_Manual. [Consultato il giorno April 2023].

[35] F. Giustino, «Band structures and Photoelectron Spectroscopy,» in *Materials Modeling using Density Functional Theory*, Oxford, Oxford University Press, 2013, pp. 152-173.

[36] J. Furthmüller e G. Kresse, «VASP the GUIDE,» Universität Wien, Wien, 2005.

[37] «Reaction path construction and determination,» March 2013. [Online]. Available: http://pfleurat.free.fr/ReactionPath.php. [Consultato il giorno April 2023].

[38] «VTST Tools - Nudged Elastic Band,» [Online]. Available: https://theory.cm.utexas.edu/vtsttools/neb.html. [Consultato il giorno April 2023].

[39] «VTST Tools - The Dimer Method,» [Online]. Available: https://theory.cm.utexas.edu/vtsttools/dimer.html. [Consultato il giorno April 2023].

[40] N. D. Mermin, «Thermal properties of the inhomogeneous electron gas,» *Phys. Rev.*, n. 137, 1965.

[41] J. Hafner, «Ab-initio simulations of materials using VASP: Density-Functional Theory and beyond,» *J Comput Chem*, vol. 29, pp. 2044-2078, 2008.

[42] S. N. Steinmann e C. Corminboeuf, «coefficient, A generalized-gradient approximation exchane hole model for dispersion,» *The Journal of Chemical Physics*, vol. 134, p. 044117, 2011.

[43] S. N. Steinmann e C. Corminboeuf, «Comprehensive benchmarking od density-dependent dispersion correction,» *Journal of Chemical Theory and Computation*, vol. 7, n. 11, pp. 3567-3577, 2011.

[44] N. Shan, M. K. Hanchett e B. Liu, «Mechanistic insights evaluating Ag, Pb an Ni as electrocatalysts for furfural reduction from first-principles methods,» *The Journal Physical Chemistry C*, vol. 121, pp. 25768-25777, 2017.

[45] X. Yuan, K. Lee, M. T. Bender, J. R. Schmidt e K.-S. Choi, «Mechanistic differences between electrochemical hydrogenation and hydrogenolysis of 5-hydroxymethylfurfural and thei pH dependence,» *ChemSusChem*, n. 15, pp. e202200952-13, 2022.

[46] J. Greeley, J. K. Norskos, L. A. Kibler, A. M. El-Aziz e D. M. Kolb, «Hydrogen Evolution Over bimetallic systems: understanding the trends,» *ChemSusChem*, vol. 7, n. 5, pp. 1032-1035.

[47] Y.-H. Fang, G.-F. Wei e Z.-P. Liu, «Constant-charge reaction theory for potential-dependent reaction kinetics at the solid-liauid interface,» *The Journal of physical chemistry C,* vol. 118, n. 7, pp. 3629-3635, 2014.

[48] Y. Kwon, K. J. P. Schouten, J. C. v. d. Waal, E. d. Jong e M. T. M. Koper, «Electrocatalytic conversion of furanic compounds,» *ACS Catalysis,* vol. 6, pp. 6704-6717, 2016.

[49] S. P. Verevkin, V. N. Emel'yanenko, E. N. Stepurko e R. V. R. D. H. Zaitsau, «Biomass-derived platform chemicals: thermodynamic studies on the conversion of 5-hydroxymethylfurfural into bulk intermediates,» *Ind. Eng. Chem. Res. 2009,* vol. 48, pp. 10087-10093, 2009.

[50] S. Pandey, M.-J. Dumont, V. Orsat e D. Rodrigue, «Biobased 2,5-furandicarboxylic acid (FDCA) and its emerging copolyesters' properties for packaging applications,» *European Polymer Journal,* vol. 160, p. 110778, 2021.